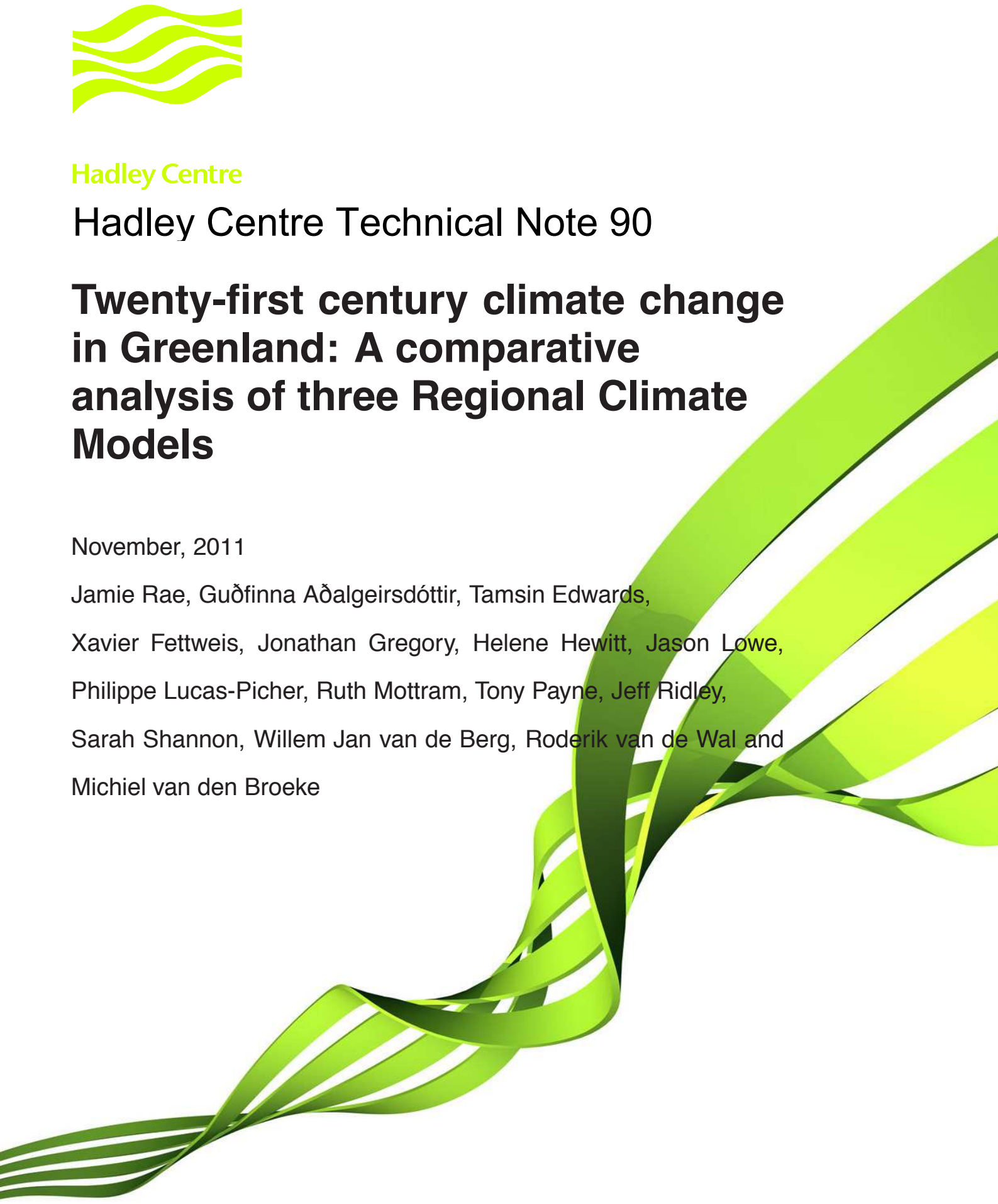

Hadley Centre

Hadley Centre Technical Note 90

Twenty-first century climate change in Greenland: A comparative analysis of three Regional Climate Models

November, 2011

Jamie Rae, Guðfinna Aðalgeirsdóttir, Tamsin Edwards, Xavier Fettweis, Jonathan Gregory, Helene Hewitt, Jason Lowe, Philippe Lucas-Picher, Ruth Mottram, Tony Payne, Jeff Ridley, Sarah Shannon, Willem Jan van de Berg, Roderik van de Wal and Michiel van den Broeke

Abstract

An assessment of high-resolution Regional Climate Model (RCM) simulations is presented for Greenland, with the aim of producing time series of surface mass balance (SMB) for the Greenland ice sheet at greater accuracy than is possible with coarser-resolution General Circulation Models (GCMs). Output from RCM simulations for the recent past is evaluated against available observations. The RCMs with state-of-the-art surface snow schemes are found to perform better than the other RCMs, highlighting the importance of such schemes for accurate projections of SMB. RCM simulations for the 21st century using SRES scenario A1B produce trends of between -5.5 and -1.1 Gt yr^{-2} in SMB.

1 Introduction

The greatest uncertainty in projections of future sea level rise is from the ice sheets of Greenland and Antarctica (*Meehl et al.*, 2007). Ice sheets contribute to sea-level rise through dynamical processes (ice flows from the interior to the coast, followed by iceberg calving) and surface mass balance (SMB; the net balance between accumulation via snowfall and ablation via melt and subsequent runoff). The accurate calculation of SMB requires a good accounting of snowfall and melt. Ice sheets are steep at the margins and flat in the high-elevation interior. Most precipitation is orographically-forced and falls at the ice sheet margins; most of the ice sheet ablation also occurs there. Most current General Circulation Models (GCMs) have insufficient resolution to represent the orography accurately at the margins of the ice sheets (see *Gregory & Huybrechts*, 2006, and references cited therein). Nevertheless, some studies using coarse-resolution GCMs, coupled to high-resolution dynamical ice sheet models, have been performed (see, e.g., *Ridley et al.*, 2005; *Mikolajweicz et al.*, 2007; *Vizcaíno et al.*, 2008, 2010). However, these studies have been limited by the low resolution of the GCMs.

To reach the high resolution necessary to resolve the steep coastal topography of the Greenland Ice Sheet (GrIS), two methods have previously been used: statistical downscaling techniques that produce higher-resolution output from the low-resolution GCM fields (e.g., *Huybrechts et al.*, 2004; *Hanna et al.*, 2005; *Gregory & Huybrechts*, 2006); and dynamical downscaling with Regional Climate Models (RCMs) at high spatial resolution, forced at the boundaries by GCMs or reanalysis products (e.g., *Box et al.*, 2004; *Fettweis et al.*, 2005; *Lefebre et al.*, 2005; *Box et al.*, 2006; *Ettema et al.*, 2009; *Ettema*, 2010; *Ettema et al.*, 2010; *Mernild et al.*, 2010). A number of RCM studies over Greenland have highlighted the importance of the resolution to reproduce the effects of the topography on the surface mass balance of the ice sheet (e.g., *Box et al.*, 2004, 2006; *Fettweis et al.*, 2005; *Lefebre et al.*, 2005; *Ettema et al.*, 2009; *Lucas-Picher et al.*, 2011). High-resolution RCMs are therefore an important tool in reducing the uncertainty in sea level rise highlighted by *Meehl et al.* (2007).

This report examines simulations conducted with RCMs for the GrIS with a view to understanding

the uncertainties in model estimates of SMB. Four RCMs (HadRM3, MAR, HIRHAM5 and RACMO2) produce simulations for the recent past, and three (HadRM3, MAR and HIRHAM5) for future scenarios. In Section 2, a brief description is given of the RCMs used, and the simulations performed. In Section 3, results are given for RCM simulations of the recent past, including evaluation against available observations. In Section 4, results are presented for future projections from the RCMs. Some conclusions are given in Section 5.

2 Model simulations

2.1 Regional Climate Models

For the future projections discussed in Section 4, we used three different RCMs: HadRM3P, HIRHAM5 and MAR. In the evaluation of simulations of the recent past, discussed in Section 3, we used an additional RCM, RACMO2. These four RCMs were all run with the same boundary conditions, and have a broadly-similar setup. The exact domain used was slightly different in each RCM. The domains used in HadRM3 and MAR were broadly similar to that shown in Fig. 1, while that used in HIRHAM5 was somewhat larger, and included more of the surrounding ocean.

2.1.1 HadRM3P

HadRM3P (*Jones et al.*, 2004), run at the Met Office Hadley Centre, is a limited-area, atmosphere-only model based on a version of the HadCM3 GCM (*Gordon et al.*, 2000) with improved atmospheric physics. An improved surface snow scheme (MOSES 2.2, see *Essery et al.*, 2001) was used. HadRM3P uses a polar rotated grid, at a resolution of 0.22° (equivalent to ∼25 km), with 19 vertical levels. The treatment of *Marshall* (1989) is used for the snow albedo.

The SMB calculated by HadRM3 in historical simulations was found to be lower than those which have generally been obtained in other studies, because of the absence of meltwater percolation and refreezing in the surface snow scheme currently in use. Refreezing was therefore calculated offline in a scheme based on the daily scheme used in the GLIMMER model (*Hagdorn et al.*, 2010), in which the refreezing is calculated as a constant multiplied by the instantaneous daily snow cover. This constant was tuned so that the annual total SMB agreed with the annual positive degree day scheme of GLIMMER (*Hagdorn et al.*, 2010), which was based on work by *Huybrechts et al.* (1991) and *Letreguilly et al.* (1991a,b), and where the maximum annual refreezing is 0.6 times the total annual snowfall.

2.1.2 HIRHAM5

The HIRHAM5 model is the hydrostatic atmospheric RCM of the Danish Meteorological Institute. HIRHAM5 is a combination of two models: the atmospheric dynamics is from the HIRLAM numerical

weather prediction model (*Eeorla*, 2006), and the physics from the ECHAM5 global model (*Roeckner et al.*, 2003). Simulations with HIRHAM5 over Greenland have been well-validated with ice core and automatic weather station data (*Mottram et al.*, 2012; *Dethloff et al.*, 2002; *Kiilsholm et al.*, 2003; *Box & Rinke*, 2003; *Stendel et al.*, 2008; *Lucas-Picher et al.*, 2011). The surface scheme in the model has been modified from ECHAM5 to account for melt and meltwater retention processes in snow, but analysis of model results suggests that some improvements are needed to produce realistic retention and refreezing of meltwater (*Mottram et al.*, 2012). The albedo of snow and ice is assumed to be a linear function of surface temperature, ranging between a mininum value (0.6) at the melting point to a maximum value (0.8) for temperatures below -5°C (*Roeckner et al.*, 2003). HIRHAM5 uses a polar rotated grid at a resolution of 0.25° (equivalent to ∼27 km) with 31 vertical levels and a timestep of 120 seconds in the dynamical scheme.

2.1.3 MAR

The MAR (Modèle Atmosphérique Régional) RCM, run at the University of Liège, is coupled to the one-dimensional surface vegetation-atmosphere transfer scheme SISVAT (Soil Ice Snow Vegetation Atmosphere Transfer) (*Gallée & Schayes*, 1994). The snow-ice component, based on the CEN (Centre d'Etudes de la Neige) snow model, CROCUS (*Brun et al.*, 1992), is a one-dimensional multi-layered energy balance model that determines the exchanges between the sea ice, the ice sheet surface, the snow-covered tundra, and the atmosphere. It includes snow thermodynamics, meltwater refreezing, snow metamorphism, snow/ice discretization, and an integrated surface albedo (*Gallée et al.*, 2001).

2.1.4 RACMO2

The Regional Atmospheric Climate Model version 2.1 (RACMO2), run at the University of Utrecht, is a combination of two numerical weather prediction models. The atmospheric dynamics originate from the High Resolution Limited Area Model (HIRLAM, version 5.0.6) (*Undén et al.*, 2002), and the physical processes are adopted from the global model of the European Centre for Medium-Range Weather Forecasts (ECMWF, updated cycle 23r4; *White*, 2004). The tuning of the model is described by *Van Meijgaard et al.* (2008). In Greenland simulations, RACMO2/GR is extended with a multi-layer snow model to represent the surface and sub-surface processes over ice sheets. This snow model includes snow/ice melt, percolation, refreezing, snow compaction, meltwater runoff, heat diffusion and determines the surface albedo using the surface snow/ice density (*Ettema*, 2010; *Ettema et al.*, 2009). *Ettema et al.* (2010) provide an evaluation of the model results.

2.2 Boundary conditions

RCMs are driven at their domain boundaries by winds, temperature, humidity and surface pressure provided from a low-resolution global model. The ocean surface is updated daily by fields of sea

surface temperature and sea ice cover. To determine the dependence of the RCM performance on boundary conditions, we conduct simulations with two different GCMs: HadCM3 (*Gordon et al.*, 2000), at a resolution of 3.75°×2.5°, with 19 vertical levels, and ECHAM5 (*Roeckner et al.*, 2003), at a resolution of ∼3.8°, also with 19 vertical levels. Simulations from the recent past (1980-1999) driven by the GCMs were supplemented by simulations driven by boundary conditions from reanalyses, namely ERA-40 (for 1980-1999) and ERA-INTERIM (for 1989-2008). The boundary conditions used in the 21$^{\mathrm{st}}$ century projections (2000-2099) came from a HadCM3 simulation with the SRES A1B scenario (*Nakicenovic et al.*, 2000), and two ECHAM5 simulations, one with SRES A1B, and one with the E1 mitigation scenario used in the ENSEMBLES project (*Lowe et al.*, 2009). All simulations, past and future, used present-day ice sheet surface topography at a resolution of ∼1 km (*Bamber et al.*, 2001), interpolated to the appropriate RCM grid.

3 Comparison and evaluation of simulations for the recent past

The future mass balance of Greenland may be estimated through simulations that incorporate likely CO_2 emissions scenarios. The uncertainty of the SMB arises from: uncertainty in future emissions (*Huybrechts et al.*, 2004); model structural differences (*Huybrechts et al.*, 2004); and parameterisation of model surface snow schemes (*Bougamont et al.*, 2007).

The reliability of climate projections from models is often assessed against the quality of present-day simulations, when evaulated against observations. In this section we compare the different RCMs aginst each other to determine if there are common failings or agreements. The particular purpose of this work is to assess the uncertainty in surface mass balance. However, SMB is not a measureable quantity and so we instead evaluate temperature, accumulation and melt.

In Section 3.1, the evaluation of surface air temperature will be discussed, followed by Sections 3.2 and 3.3, net accumulation and surface melt. Finally, in Section 3.4, the SMB itself will be evaluated.

3.1 Surface air temperature (T_{as})

The surface air temperatures (T_{as}) obtained from the historical-period RCM simulations, are assessed aginst the Danish Meteroological Institute (DMI) synoptic weather stations situated around the Greenland coast (*Cappelen*, 2011), and the Automatic Weather Stations (AWS) of the GC-Net network (*Box & Steffen*, 2000), shown on the map in Fig. 1. Precise locations can be found in the table on p39 of *Cappelen et al.* (2000), and in Table 1 of *Box & Steffen* (2000).

To perform the evaluation, the T_{as} fields from the models were interpolated to the locations of the observing sites as follows:

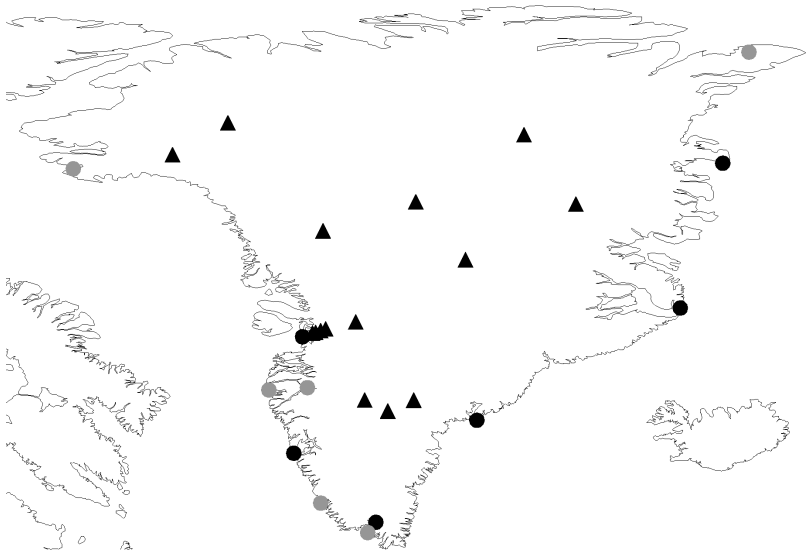

Figure 1: Observing stations used in the $T_{\rm as}$ evaluation. Black circles represent DMI stations that were used in the evaluation of RCM simulations forced by HadCM3, ECHAM5 and ERA40. Grey circles are those that were used in the evaluation of all simulations, including those forced by ERA-Interim. The reasons for this difference are explained in the text. Triangles represent GC-Net stations.

1. The model $T_{\rm as}$ field was interpolated, by 2-D bilinear interpolation, to the longitude and latitude of the observing site.

2. The orography field was also interpolated, by 2-D bilinear interpolation, to the longitude and latitude of the observing site.

3. The nearest model gridbox to the site was determined.

4. A lapse rate was calculated using the modelled $T_{\rm as}$ in, and the elevations of, that gridbox and the eight surrounding gridboxes (neglecting ocean gridboxes).

5. The calculated lapse rate was used, along with the interpolated orography and the published elevation (above mean sea level) of the observing site, to apply a vertical correction to $T_{\rm as}$ calculated by 2-D interpolation. The size of this correction depends on the location of the observing site, and on the difference between the elevation of the gridbox and that of the observing site, but can be as much as 3°C.

In Fig. 2, we plot 20-year mean modelled $T_{\rm as}$ against available observations for each observing station. For DMI coastal stations, long term observations are available, although for this analysis only 6 stations had data after the year 2000. Twenty-year means of modelled $T_{\rm as}$ are evaluated against the corresponding years in the observations (1989-2008 for the ERA-Interim-forced simulations, and 1980-1999 for the others). This means that ERA-Interim-forced simulations are only evaluated against observations from 6 stations (the grey circles in Fig. 1), whereas the other simulations are evaluated against 12 stations (all circles, grey and black, in Fig. 1). For GC-Net stations,

observations are only available from the mid-1990s onwards, and all simulations are evaluated against the mean observations for the period for which they are available; this period depends on the period for which each AWS was operational.

The correlations between modelled and observed 20-year mean $T_{\rm as}$, and the mean and RMS errors of the model output relative to observations, are given in Table 1. It can be seen from Fig. 2 and Table 1 that for most models there is better correlation with observations in the interior than on the coast; this may be because of errors introduced by the surface physics scheme, or due to limited model resolution conflicting with complex orography and meteorology near coastal stations. On the other hand, the $T_{\rm as}$ on the ice sheet are functions simply of elevation, insolation and mean aerodynamic flow, leading to a noticeable improvement in the correlation.

At the coastal stations, HadRM3 (Fig. 2a) generally has a cold bias regardless of the simulation (Table 1). Additionally, in Fig. 2b, we see that for the stations in the percolation zone, HadRM3 underestimates $T_{\rm as}$ when the observed $T_{\rm as}$ is above freezing point. This is because the physics scheme melts ice corresponding to the diagnosed excess temperature above freezing, then resets the surface temperature to freezing.

In Fig. 3, we show the geographical distribution of $T_{\rm as}$ in MAR forced by boundary conditions from ECHAM5, and the difference between this and $T_{\rm as}$ in the equivalent HadRM3 and HIRHAM5 simulations. The observing stations used for the $T_{\rm as}$ evaluation are also shown (circles for DMI stations; triangles for GC-Net). It can be seen that $T_{\rm as}$ in HadRM3 is considerably lower ($\sim$8°C) than that in MAR on the ice-free areas around the coast (as seen in Fig. 2), the reasons for which are not evident. Both HadCM3 and HIRHAM5 are warmer than MAR in the interior, in some regions by 3-4°C, and yet the RMS errors are similar. The 3 GC-Net stations where HadRM3 failed to produce $T_{\rm as}$ above freezing point (Fig. 2b) can be seen close to the west coast.

There is no correlation between modelled and observed $T_{\rm as}$ at coastal stations for most HadRM3 simulations (Table 1); the mean and RMS errors are also greater in HadRM3. In Table 1, MAR and HIRHAM5 have better model-observation correlation and lower mean and RMS errors; this can also be seen in Fig. 2. The ERA40-forced RACMO2 simulation performs better than the equivalent HadRM3 and MAR simulations in terms of correlation and bias.

3.2 Accumulation

We assess the model estimates of accumulation, i.e. total precipitation minus evaporation ($P - E$), by comparison with observations. The observational dataset – shallow ice cores and stakes – comprises 263 published and unpublished observations from *Reeh* (1991), *Bales et al.* (2009), *Cogley* (2004) and *van de Wal et al.* (2005). Model and observations are matched by elevation and time period. Since we are considering annual net accumulation, we neglect observations in the ablation zone. We use an improved version of the method as used by *Rignot et al.* (2008), which is described in detail by *van de Berg et al.* (2012).

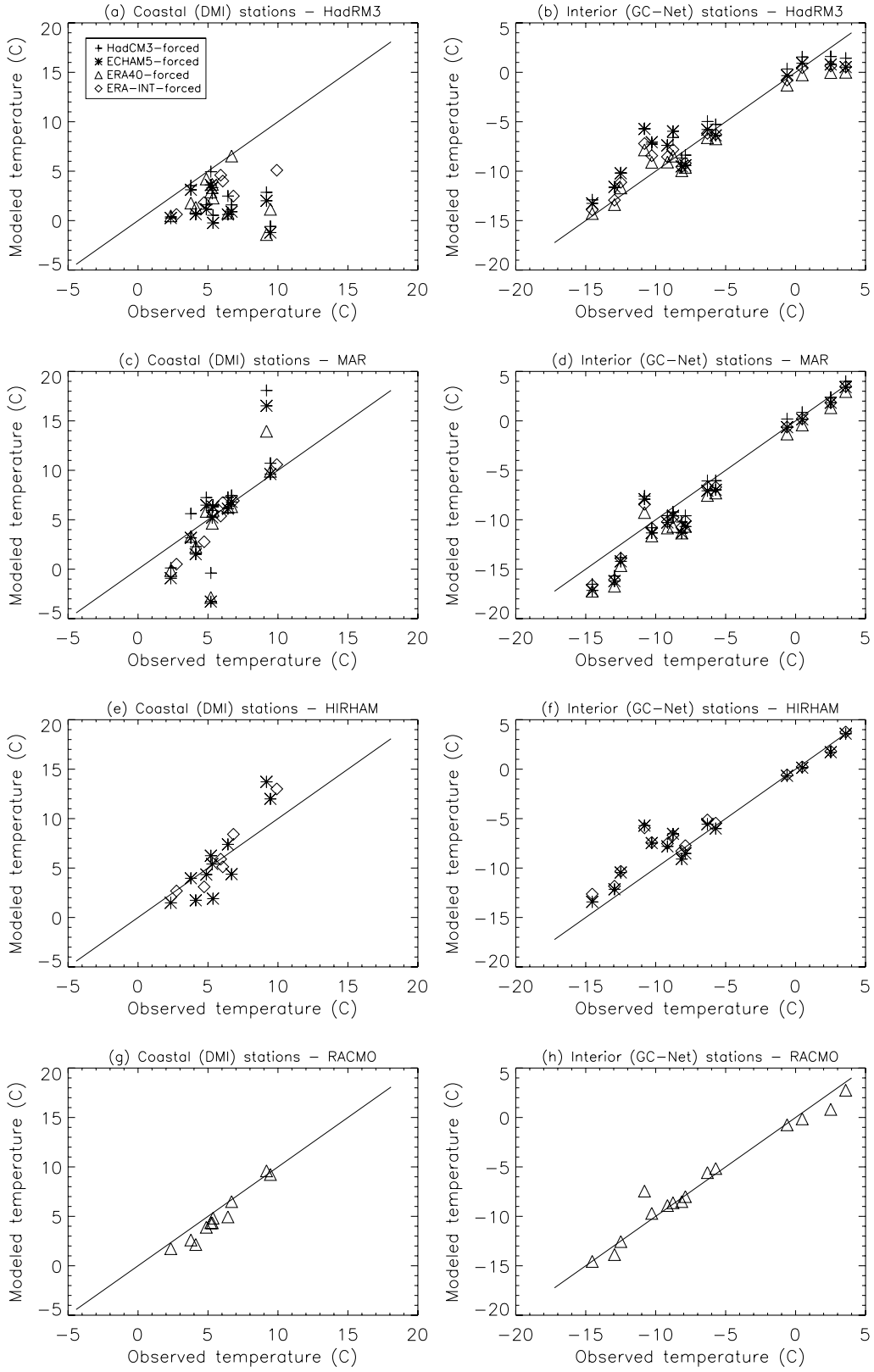

Figure 2: Modelled versus observed summer (JJA) T_{as} (°C). Each point represents an observing station. Left column: Coastal (DMI) stations. Right column: Interior (GC-Net) stations. From top: HadRM3, MAR, HIRHAM5, RACMO2. The line of 1:1 correspondence is also shown.. Legend (given in (a)) is the same in all figures.

Table 1: Correlations between modelled and observed summer (JJA) surface air temperatures $T_{\rm as}$, and RMS errors in modelled $T_{\rm as}$ (K) relative to observations.

Simulation	Coastal (DMI) stations			Interior (GCNet) stations		
	Correlation	Mean error	RMS error	Correlation	Mean error	RMS error
HadCM3-forced HadRM3	-0.09	-3.82	4.66	0.96	1.13	2.05
ECHAM5-forced HadRM3	-0.24	-4.41	5.23	0.93	0.71	2.21
ERA40-forced HadRM3	-0.17	-3.55	4.73	0.97	-0.49	1.61
ERAINT-forced HadRM3	0.82	-2.92	3.18	0.97	0.05	1.57
HadCM3-forced MAR	0.82	0.73	3.47	0.98	-0.45	1.48
ECHAM5-forced MAR	0.80	-0.47	3.66	0.97	-1.13	1.87
ERA40-forced MAR	0.81	-0.67	3.01	0.98	-1.62	2.03
ERAINT-forced MAR	0.98	-0.55	1.29	0.98	-0.94	1.58
ECHAM5-forced HIRHAM5	0.89	-0.02	2.20	0.96	0.87	1.81
ERAINT-forced HIRHAM5	0.96	0.34	1.61	0.97	1.16	1.83
ERA40-forced RACMO2	0.98	-0.78	1.00	0.98	0.06	1.08

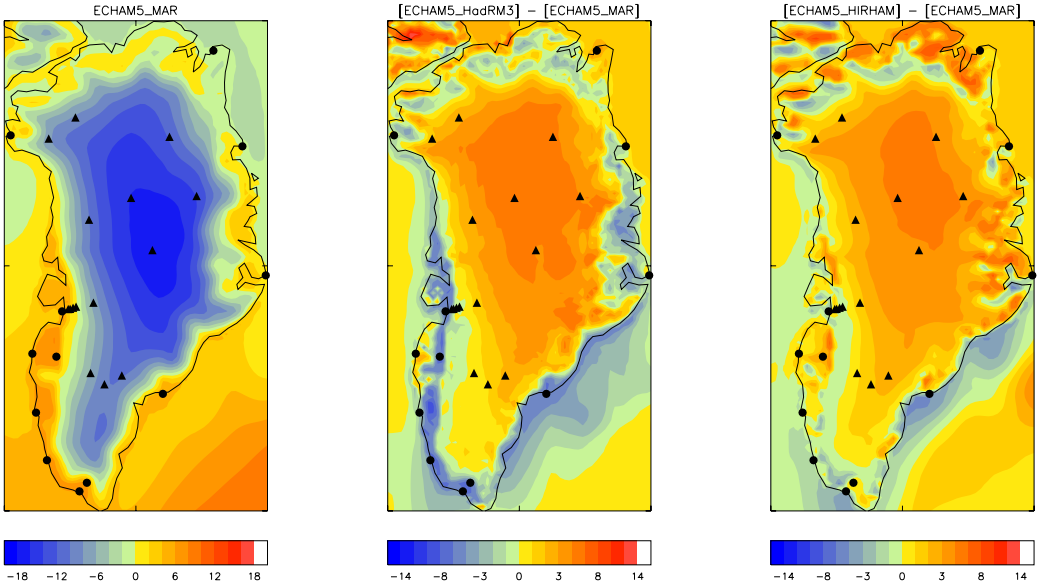

Figure 3: Surface air temperatures ($T_{\rm as}$). Left: ECHAM5-forced MAR. Centre: Difference between ECHAM5-forced HadRM3, and ECHAM5-forced MAR. Right: Difference between ECHAM5-forced HIRHAM5, and ECHAM5-forced MAR. Observing stations used in the $T_{\rm as}$ evaluation are also shown (circles for DMI stations; triangles for GC-Net)

This method estimates the random and systematic model errors of $P - E$. The systematic error is comprised of a fixed and functional (e.g. one that increases linearly with $P - E$) components. A Gaussian distribution for the random error is applicable for $\delta(P - E)_{\rm bc}$, the deviations of the bias-corrected model values from observation, normalised by observation and model standard deviations. An optimal estimate of the random and systematic error is archived if $\delta(P - E)_{\rm bc}$ is normally-distributed around zero with a standard deviation of unity. This optimal estimate is found by minimising the deviations from the desired distribution. We set the observational error ($\mathrm{SMB}_{\rm obs}$) to be 10.0 + 0.05$\times\mathrm{SMB}_{\rm obs}$ millimetres water equivalent per year (mmWE yr^{-1}). Model errors are spatially correlated, reducing the degrees of freedom when calculating the error for the whole ice sheet. We assume that all the models have an autocorrelation length of 200 km.

The total mass flux onto the ice sheet, for each model and forcing scenario, is shown in Fig. 4. For HIRHAM5 and HadRM3, the reanalysis-driven simulations have a smaller total error than the GCM-driven simulations, mainly due to smaller biases. For all RCMs, in reanalysis-driven simulations the uncertainty due to random errors is smaller than that in GCM-driven simulations. After correction for systematic errors, the model estimates are surprisingly similar, except for those from from MAR. This deviation is due to the much lower $P - E$ rates MAR predicts for high-accumulation areas like south-east Greenland or along the Lauge Koch Kyst. The lack of observations for the locations with highest predicted $P - E$ allows this spread in bias-corrected $P - E$.

In general, the uncertainty is about 20% of the total accumulation, which is mainly due to model biases. The accumulation is in general underestimated in GCM-driven simulations. Since reduction

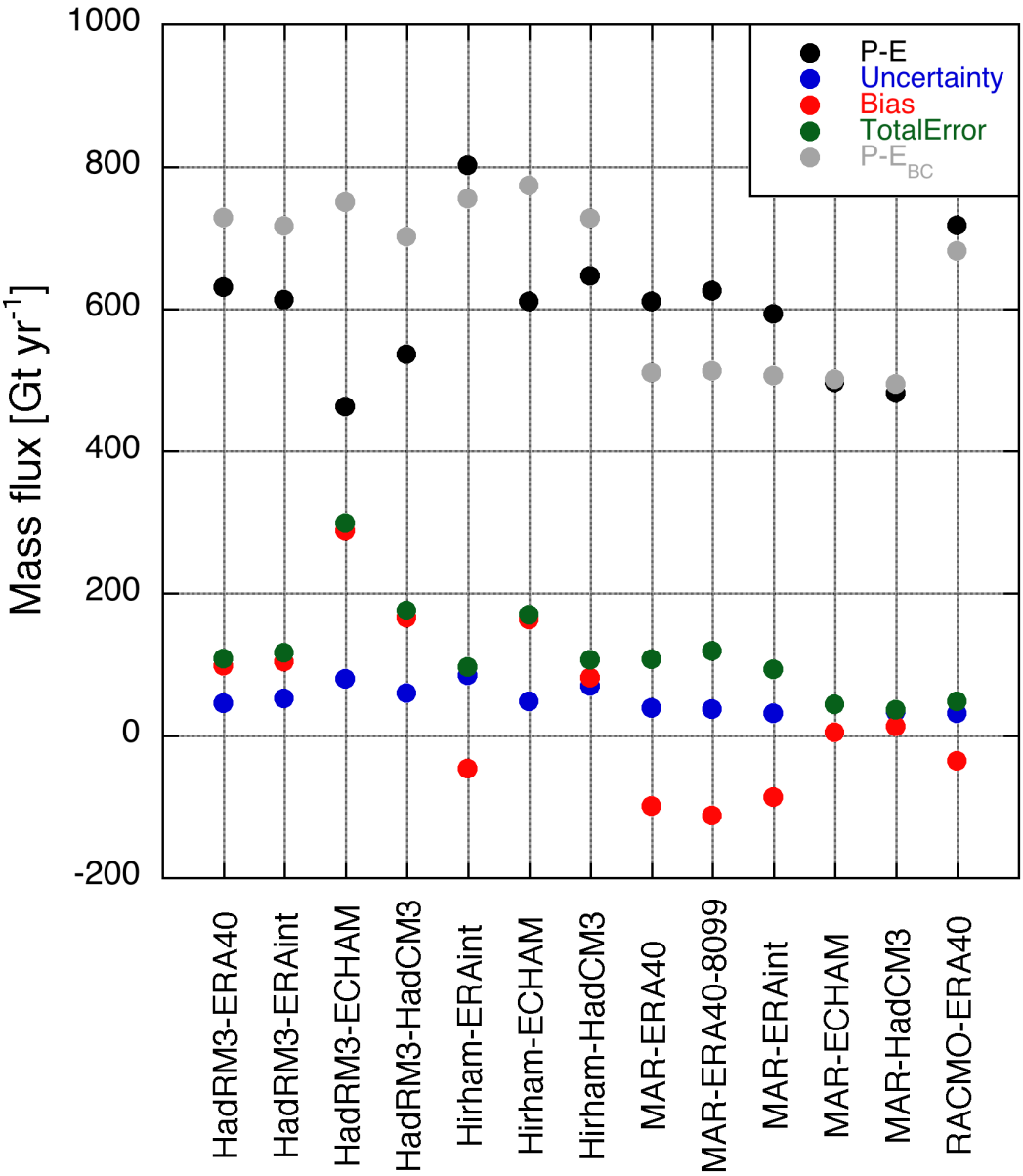

Figure 4: Uncertainty estimates for all present-day climate simulations integrated for the GrIS. $P-E$ is the uncorrected model estimate; Uncertainty is the integrated random error; Bias the integrated systematic error; TotalError is the root-mean square sum of the uncertainty and bias; $(P-E)_{BC}$ is the bias corrected model estimate.

of accumulation has an enhancing effect on snowmelt, this accumulation underestimation implies that the RCM projections of future climate might overestimate the increase in melt in a warmer climate in the future.

3.3 Melt area extent and meltwater production

Since ablation is a key factor in the Greenland surface mass balance, a good representation of melt and meltwater production is essential. The spaceborne passive microwave brightness temperature dataset offers an opportunity to evaluate the daily melt extent simulated by the RCM at the scale of the whole ice sheet, at a horizontal spatial resolution of 25 km. In addition, with more than 30 years of data, this dataset allows us to evaluate the interannual variability of the melt in the models. Although the microwave data set can be used for a direct evaluation of the surface mass balance simulated by the model, biases in simulated precipitation and meltwater amount impact the comparison of the melt extent and explain most of the disagreements with the satellites as shown by *Fettweis et al.* (2011).

The RCM output and satellite data were interpolated onto the 25 km MAR grid. For consistency with the rest of the analysis, the meltwater production over the ice sheet is calculated using the RACMO2 ice sheet mask. Melt is assumed to have taken place if the daily melt rate is above a certain threshold. These thresholds, different for different RCMs and given in Table 2, have been chosen to compare best with the satellite-derived melt extent using the T19Hmelt algorithm (*Fettweis et al.*, 2011).

The temperature threshold for melt (T19H > 227.5 K) used in the satellite data was constrained with daily surface air temperature > 273.15 K from GC-Net mesurements. No observations of meltwater production are available, so meltwater thresholds were derived from this temperature threshold for each of the models; these thresholds are necessarily model-dependent. The meltwater production, and therefore the melt threshold, are particularly sensitive to the surface albedo used in the models. For given atmospheric and snowpack conditions, a higher albedo leads to a lower meltwater threshold, and vice versa. Results for the comparison of MAR and RACMO2 with T19HMelt can be found in *Fettweis et al.* (2011). The albedo in HIRHAM5 is lower than that in MAR and RACMO2 in the percolation zone (over melting snow); hence, HIRHAM5 has a higher melt threshold than MAR or RACMO2. HadRM3 has a higher surface albedo everywhere than the other 3 models; it therefore has the lowest melt threshold of all.

In Table 2, the meltwater thresholds are listed for the various models. Those for MAR and RACMO2 are the same as in *Fettweis et al.* (2011). In Fig. 5, we show the seasonal cycle in the 20-year mean total melt area over the ice sheet, for all 4 RCMs as well as the satellite data (labelled T19Hmelt). It can be seen that both HadRM3 and HIRHAM5 overestimate the melt extent at the beginning of the season and underestimate it at the end. The early start of the melt season in HIRHAM5 is due to the snow albedo decreasing too quickly at the end of spring, which enhances

Table 2: Thresholds for melt event detection

Data/RCM	Forcing	Melt threshold
Satellite T19Hmelt		T19H > (227.5±2.5) K
MAR	ERA-Interim	Melt > (8.25±0.75) mmWE day^{-1}
RACMO2	ERA-40	Melt > (8.25±0.75) mmWE day^{-1}
HIRHAM5	ERA-Interim	Melt > (10.50±0.75) mmWE day^{-1}
HadRM3	ERA-Interim	Melt > (5.00±0.50) mmWE day^{-1}

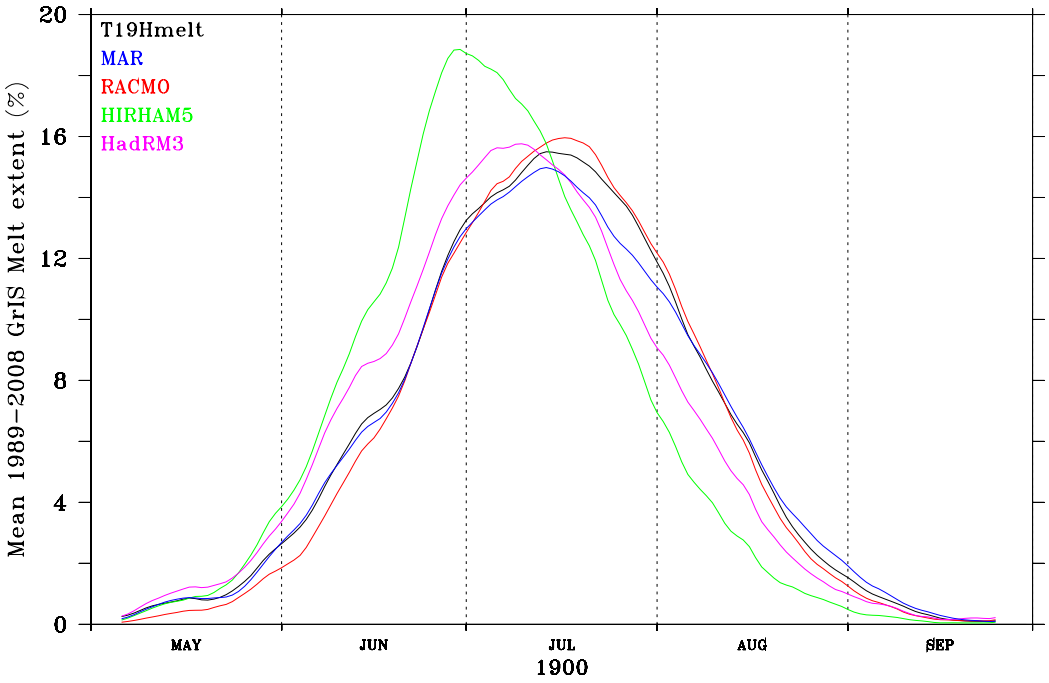

Figure 5: Mean seasonal cycle (1989-2008) of melt area (in % of ice sheet area) simulated by the 4 RCMs as well as retrieved from the spaceborne passive microwave data set with the T19Hmelt algorithm.

Table 3: Comparison between satellite-based and RCM-based melt detection. RMSE is RMS error of RCM melt extent time series relative to satellite melt extent time series. Correlation is between RCM and satellite melt extent time series

Model	Percentage of 25 km gridboxes where melt is detected by				RMSE	Correlation
	RCM and satellite	RCM but not satellite	Satellite but not RCM	Neither satellite nor RCM		
MAR	3.8	1.9	2.0	92.3	2.8	0.92
RACMO2	3.7	2.0	2.1	92.2	2.9	0.92
HIRHAM5	3.4	2.5	2.4	91.7	4.8	0.81
HadRM3	3.8	1.9	1.9	92.4	3.1	0.91

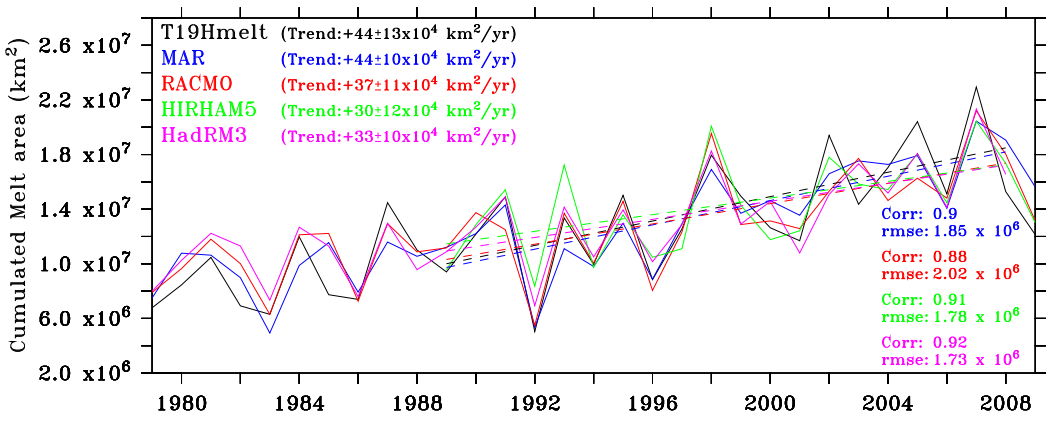

Figure 6: Time evolution of the annual total ice sheet melt area simulated by the RCMs and retrieved from T19Hmelt. The total melt area is defined as the annual total sum of every daily ice sheet melt area. The ERA-40 forced simulations are used before 1989.

the melt. In Table 3, we give a statistical comparison of the RCM output with the satellite data. The RMS error in the RCM output relative to the satellite data gives an indication of the daily variability; except in the case of HIRHAM5, there is good comparison. For MAR, RACMO2 and HadRM3, the correlation between the RCM daily melt extent and that from the satellite data is greater than 0.9. The time series for the total melt area (Fig. 6) for all four RCMs shows that despite errors in the phase of the annual melt cycle the models reproduce the observed interannual variability and trend in the total melt extent.

3.4 Surface mass balance (SMB)

Surface mass balance (SMB) is defined as the difference between accumulation and ablation, i.e. precipitation minus the sum of runoff, sublimation and evaporation. The SMB can be generated, from the appropriate RCM diagnostics (Fig. 9), as an annual and area mean time series. Here we compare the RCMs with previous estimates from *Box et al.* (2006), *Hanna et al.* (2008), *Fettweis et al.* (2008) and *Wake et al.* (2009). All of these are inferred from model simulations forced with

Maps of 20-year (1989-2008) mean summer meltwater production for all RCMs are shown in Fig. 7. The maximum melt in MAR and RACMO2 occurs in the low-elevation coastal ablation zone. This pattern is a response to their snow schemes (see Fig. 8) which allow all snow cover to melt, exposing low albedo bare ice in summer. Since neither HIRHAM5 or HadRM3 have an adequate snow physics scheme, their snow albedo only changes as a function of the local air temperature. With a high sensitivity of albedo to temperature, HIRHAM5 can produce a high surface melt rate as indicated in Fig. 7 and Table 2, but cannot reporduce the annual cycle (Table 3). On the other end of the scale, the HadRM3 albedo scheme has a low sensitivity to surface temperature, and consequently shows little reduction in albedo, and weak melt along the ice sheet margins. The selection of melt thresholds (Table 2) allows HadRM3 to compare well in melt extent with the other models (Fig. 6) but will result in a high surface mass balance.
We shall see, in Section 3.4, that an essential component of a good snowpack scheme is its ability physically to simulate refreezing of some of the surface melt. Such refreezing releases latent heat and warms the snow. It is speculated that the loss of embedded snowpack heat in autumn may contribute to extending the surface melt season. The lack of a snowpack model in HIRHAM5 and HadRM3 may explain the early dropoff in melt extent compared with MAR and RACMO2.

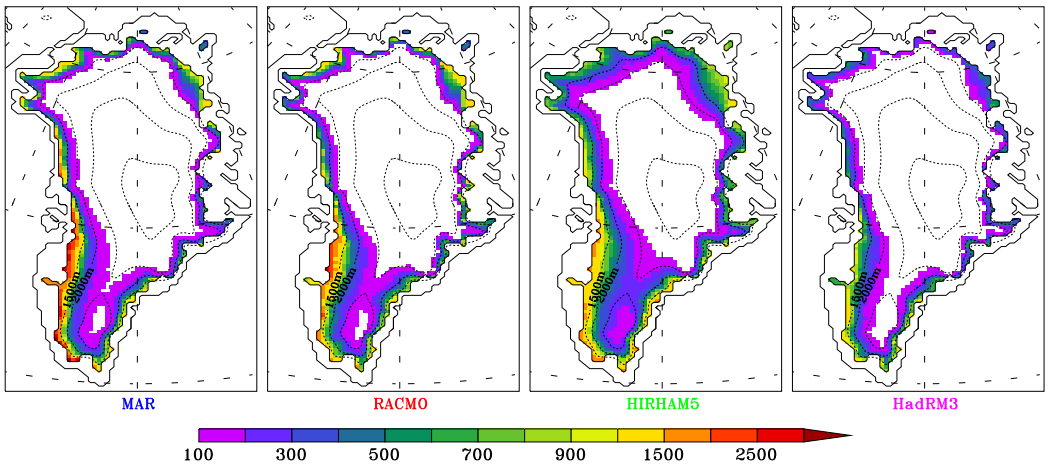

Figure 7: The average summer meltwater production in mmWE per summer, simulated by the 4 RCMs over 1989-2008.

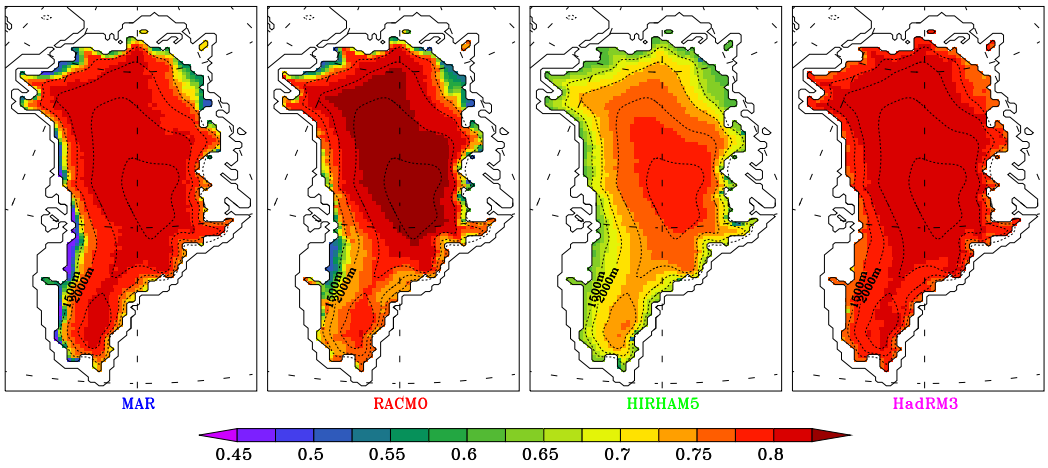

Figure 8: The 1989-2008 mean July albedo simulated by the 4 RCMs. The monthly mean July albedo is shown here because the minimum of albedo occurs during this month corresponding to the maximum extent of the bare ice area.

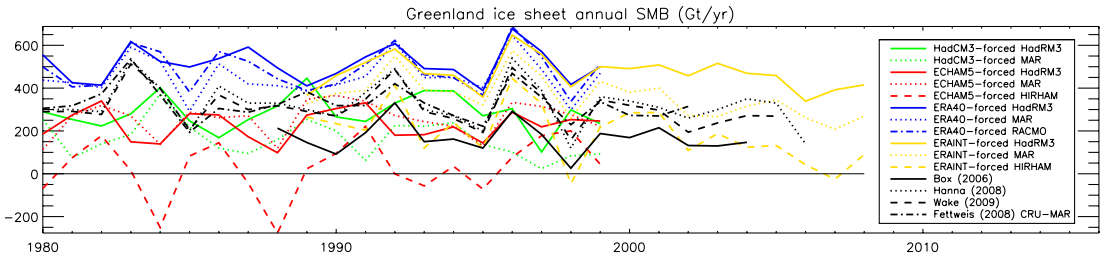

Figure 9: Time series for GrIS annual SMB (Gt yr^{-1}) in the historical RCM runs (red, yellow, green, and blue lines), compared with published results (black lines).

reanalaysis datasets. This is neccessary since estimates of the total mass balance of the icesheets, cannot disentangle the ice-dynamic and surface components The range of the previous estimates is similar to those from the RCMs when forced by ERA-Interim, with the exception of HadRM3, which we know produces a low surface melt (Fig. 7).

In Fig. 9, the estimates of *Box et al.* (2006), *Hanna et al.* (2008), *Fettweis et al.* (2008) and *Wake et al.* (2009) are seen to produce time series which are temporally similar to each other, but different from those of the RCM simulations. These previously-published estimates are all produced by models driven by reanalysis data, and indeed many features of their interannual variability also appear in the SMB from the reanalysis-driven simulations presented here. The mean SMB in the reanalysis-driven MAR and HIRHAM5 simulations is also similar to that in the previously-published estimates, while HadRM3 is more of an outlier. HIRHAM5 has the highest interannual variability in the reanalysis-forced simulations, which is likely related to its low surface albedo. The spread in SMB in the various RCM simulations in Fig. 9, and the differences from the previously-published estimates, is indicative of systematic errors in the GCMs whose output was used for boundary conditions, as well as in the RCMs themselves.

Also from Fig. 9, it can be seen that the interannual variability in the SMB from the RCM runs is determined mainly by the boundary conditions (different RCMs with the same boundary conditions have similar variability). The mean SMB, however, depends on both the RCM and the boundary conditions. In general, the GCM-driven historical simulations tend to give lower SMB than the equivalent reanalysis-driven simulations. However, for MAR the HadCM3 forcing produces a lower mass balance than ECHAM5 forcing, but for HIRHAM5 and HadRM3 the ECHAM5 forcing produces the lower mass balance. For HIRHAM5 the SMB goes negative when forced by ECHAM5. The precipitation and runoff timeseries (Fig. 10) reveal that the GCM-driven simulations have less precipitation and more runoff than the corresponding reanalysis-driven simulations, leading to the lower SMB. Whereas MAR and HadRM3 produce similar precipitation for each GCM forcing, the precipitation is significantly greater in HIRHAM5. An explanation for this may be in that the HIRHAM5 domain is much more extensive that that of MAR and HadRM3, which will allow it to gain water vapour from the local ocean in excess of that provided from the boundary conditions. Thus HIRHAM5 physics will

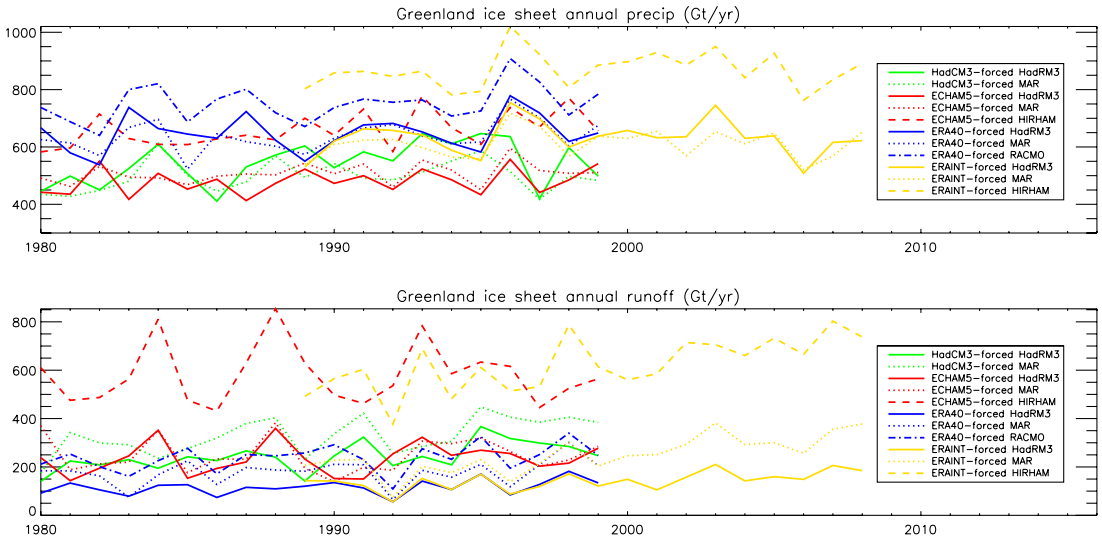

Figure 10: Time series for total GrIS precipitation and runoff in the historical RCM simulations

have more influence on atmospheric properties over Greenland than permitted within the smaller domains of MAR or HadRM3 seen in Fig. 9. It can also be seen in Fig. 10 that HIRHAM5 has a very high runoff, probably due to its low albedo and because meltwater retention and refreezing are not adequately represented in that model.

A map of SMB (Fig. 11) is shown for MAR forced by ERA40 boundary conditions; maps are also shown for the difference in SMB between this simulation and the MAR simulations forced by boundary conditions from HadCM3 and ECHAM5. The mass balance is strongly positive on the east coast and negative on the west. It can be seen that the SMB in the GCM-forced simulations is less than that in the ERA40-forced simulations almost everywhere, but notably at the ice sheet margins. The ECHAM5-forced simulation produces a very high precipitation on the south-east tip of Greenland, and a slightly higher mass balance in the north.

A summary of area average, 20-year mean, mass balances for the historical period (Fig. 9) is shown for all the historical RCM simulations in Table 4, along with trends and interannual standard deviations. Equivalent numbers for the previously-published time series are shown in Table 5. Trends which over 20 years exceed the standard deviation are highlighted in bold. It can be seen that in most cases the 20 year trend is not significant. The exceptions are HadCM3-forced MAR, ERA-INT-forced MAR and ERA-INT-forced HIRHAM5. In an attempt to determine the reason for this, 20-year means, standard deviations and trends are shown for total precipitation (solid and liquid) in Table 6, and for runoff in Table 7. In the case of HadCM3-forced HadRM3, the 20 year trends in these two fluxes are significant, but the two trends cancel to give a negligible trend in SMB. For all other simulations where the trend in SMB is not significant, the trend in one or both of precipitation and runoff is not significant; in a number of cases, this is exacerbated by the competing trends being of similar magnitude.

Time series for refreezing of meltwater are shown in Fig.12 for HadRM3, MAR and RACMO2.

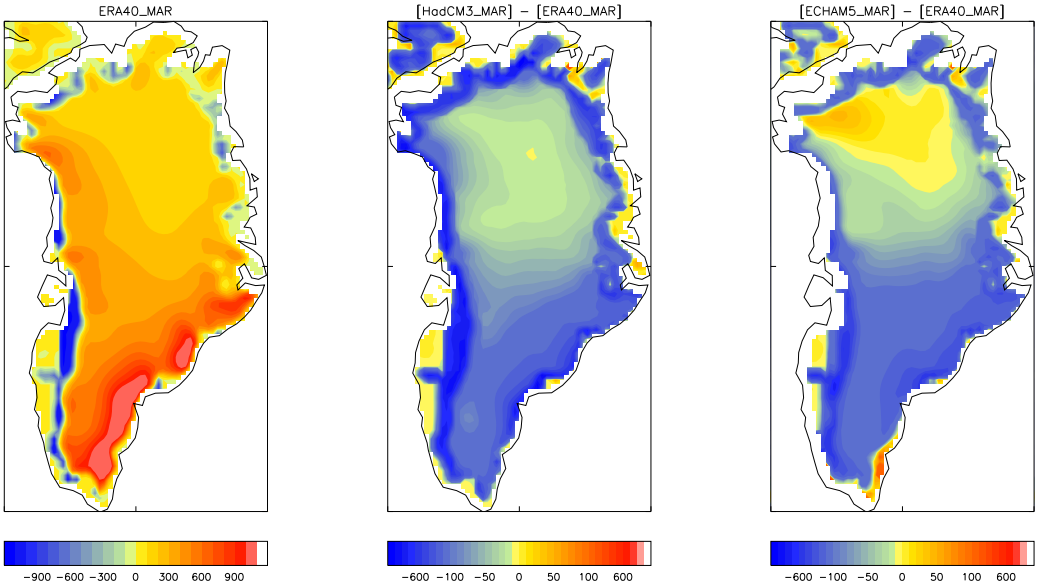

Figure 11: Surface mass balance (SMB), in mmWE yr^{-1}. Left: ERA40-forced MAR. Centre: Difference between HadCM3-forced MAR, and ERA40-forced MAR. Right: Difference between ECHAM5-forced MAR, and ERA40-forced MAR.

Table 4: 20-year means, standard deviations and trends in SMB in historical simulations. The values for the HadCM3-, ECHAM5- and ERA40-forced simulations are for 1980-1999; for the ERA-INT-forced simulations they are for 1989-2008. Trends which over 20 years exceed the standard deviation are highlighted in bold.

Boundary Conditions	RCM	20-year mean (Gt yr^{-1})	Standard Deviation (Gt yr^{-1})	Trend (Gt yr^{-2})
HadCM3	HadRM3	285	81	-0.35
	MAR	163	85	**-5.35**
ECHAM5	HadRM3	228	69	+0.30
	MAR	256	78	+2.06
	HIRHAM5	30	134	+5.28
ERA40	HadRM3	511	78	+0.22
	MAR	455	91	+0.90
ERA-INT	HadRM3	469	77	-3.10
	MAR	359	95	**-8.76**
	HIRHAM5	189	130	**-11.28**

Table 5: As table 4, but for previously-published time series.

Published time series	Mean (Gt yr^{-1})	Standard Deviation (Gt yr^{-1})	Trend (Gt yr^{-2})
Box et al. (2006)	170	71	-2.52
Hanna et al. (2008)	324	100	-2.75
Wake et al. (2009)	310	327	-2.95
Fettweis et al. (2008) CRU-MAR	-49	90	-2.44

Table 6: 20-year means, standard deviations and trends in total precipitation (solid and liquid) in historical RCM simulations. The values for the HadCM3-, ECHAM5- and ERA40-forced simulations are for 1980-1999; for the ERA-INT-forced simulations they are for 1989-2008. Trends which over 20 years exceed the standard deviation are highlighted in bold.

Boundary Conditions	RCM	20-year mean (Gt yr^{-1})	Standard Deviation (Gt yr^{-1})	Trend (Gt yr^{-2})
HadCM3	HadRM3	544	74	**+5.06**
	MAR	499	53	+1.93
ECHAM5	HadRM3	480	44	+2.15
	MAR	508	35	**+1.87**
	HIRHAM5	659	61	**+4.99**
ERA40	HadRM3	648	62	+1.93
	MAR	636	54	**+3.34**
ERA-INT	HadRM3	632	61	+0.21
	MAR	611	50	+0.65
	HIRHAM5	868	63	+1.70

Table 7: 20-year means, standard deviations and trends in total runoff in historical RCM simulations. The values for the HadCM3-, ECHAM5- and ERA40-forced simulations are for 1980-1999; for the ERA-INT-forced simulations they are for 1989-2008. Trends which over 20 years exceed the standard deviation are highlighted in bold.

Boundary Conditions	RCM	20-year mean (Gt yr^{-1})	Standard Deviation (Gt yr^{-1})	Trend (Gt yr^{-2})
HadCM3	HadRM3	243	56	**+5.48**
	MAR	329	74	**+7.31**
ECHAM5	HadRM3	234	63	+1.91
	MAR	250	69	-0.08
	HIRHAM5	581	121	-0.19
ERA40	HadRM3	117	31	**+1.92**
	MAR	178	53	+2.53
ERA-INT	HadRM3	143	38	**+3.37**
	MAR	248	77	**+9.48**
	HIRHAM5	622	111	**+12.75**

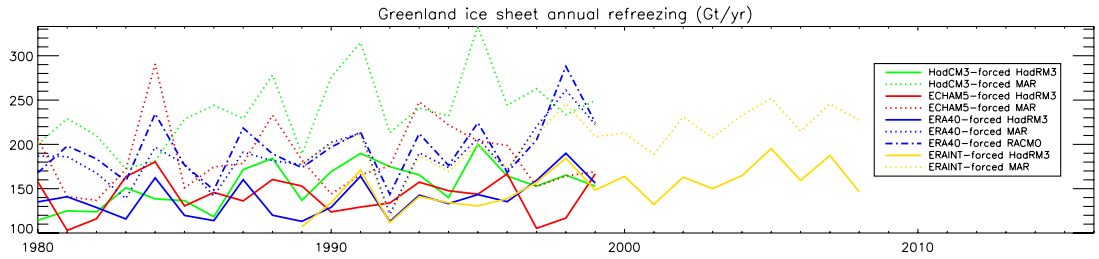

Figure 12: Time series for GrIS annual refreezing (Gt yr^{-1}) in the historical RCM runs for HadRM3 (refreezing calculated offline - see Section 2.1.1), MAR and RACMO2

Table 8: 20-year means, standard deviations and trends refreezing in historical simulations. HadRM3 and HIRHAM5 do not simulate refreezing, but refreezing was calculated offline for HadRM3 (see Section 2.1.1). Trends which over 20 years exceed the standard deviation are highlighted in bold.

Refreezing				
Boundary Conditions	RCM	20-year mean (Gt yr^{-1})	Standard Deviation (Gt yr^{-1})	Trend (Gt yr^{-2})
HadCM3	HadRM3	154	24	**+2.35**
	MAR	238	41	**+3.41**
ECHAM5	HadRM3	142	22	+0.01
	MAR	186	39	+0.16
ERA40	HadRM3	139	21	**+1.48**
	MAR	186	32	**+2.50**
ERA-INT	HadRM3	151	23	**+2.37**
	MAR	206	32	**+3.49**

Meltwater retention and refreezing are not represented in HadRM3, nor are they adequately represented in HIRHAM5. However, refreezing was calculated offline for HadRM3 as described in Section 2.1.1. This was not done for HIRHAM5. It can be seen in Fig. 12 that the refreezing calculated offline for HadRM3 tends to be lower than that calculated online in MAR. 20-year means, standard deviations and trends are shown for refreezing in Table 8. Again, it can be seen that HadRM3 has lower refreezing than MAR. There is also less variability (given by the standard deviation) in the offline HadRM3 refreezing than in the online refreezing from MAR. As in the case of the runoff in Table 7, the trend in the refreezing, taken over 20 years, is always greater than the standard deviation, except when the models are forced by boundary conditions from ECHAM5.

The evaluation of model SMB in the ablation zone is difficult because few long in-situ observational records exist. Here, RCM SMB from 3 RCMs - HadRM3, MAR and HIRHAM5 - is compared with observations from 5 field sites from the K-transect in western Greenland (*van de Wal et al.*, 2005). Only sites located on the ice sheet itself have been used. The observations provide a useful tool to evaluate whether the RCMs can predict the transition from ablation zone to accumulation zone.

Table 9: Correlation coefficients and normalised root mean square error for simulated and observed SMB. Annual SMB has been averaged over the evaluation period.

Boundary conditions	RCM	Evaluation period	r	NRMSE
ERA-Interim	MAR	1991-2010	0.96	0.40
	HIRHAM5	1991-2009	0.99	1.02
	HadRM3	1991-2008	0.95	2.61
ECHAM5	MAR	1991-2010	0.96	0.51
	HIRHAM5	1991-2010	0.99	1.06
	HadRM3	1991-2010	0.96	1.71
ERA-40	MAR	1991-2001	0.98	0.23
	HadRM3	1991-2001	0.93	3.05
HADCM3	MAR	1991-1999	0.94	0.87
	HIRHAM5	1991-1999	0.99	0.78
	HadRM3	1991-1999	0.93	1.36

In Fig. 13, we show scatter plots of the simulated multiannual mean SMB against observations for each of the sites. The pattern of underestimation at some sites and overestimation at others is strongly dependent on which RCM is used, and less dependent on the choice of forcing. HadRM3 and HIRHAM5 tend to underestimate the SMB at sites S6, S7 and S8 (i.e. closest to the ice-sheet margin), and overestimate at S9 and S10 (further away from the margin), while MAR has a general tendency to overestimate at all sites.

In Table 9, correlation coefficents between modelled and observed SMB, averaged over the evaluation period, are given for each simulation. Normalised root-mean-square errors (NRMSE) of modelled relative to observed SMB are also given. The results for NRMSE corroborate those seen in previous sections, which suggest that, of the three RCMs, MAR performs best and HadRM3 worst, but all 3 models have similar correlations.

4 Projections for the 21st century

4.1 Surface air temperature ($T_{\rm as}$)

Fig. 14 shows the time series of ice sheet mean summer (JJA) $T_{\rm as}$ for the 3 RCMs, forced by ECHAM5-A1B boundary conditions. As seen in the historical simulations, $T_{\rm as}$ in MAR is 2°C lower than in the other 2 RCMs, probably because of differences in boundary layer processes and in the treatment of surface turbulent fluxes. This may in turn be caused by differences in latent heat fluxes because of differences in melt rates, due to different treatments of albedo. However, there is a general upward trend in all models, giving temperarture increases of $\sim$4°C between 2000 and 2099. The effect of varying boundary conditions on the output of a single RCM can be seen in Fig. 15, which shows time series for MAR forced by each of the 3 sets of boundary conditions (HadCM3-A1B, ECHAM5-A1B and ECHAM5-E1). MAR was chosen for this analysis because it is the only one of the 3 RCMs to include a full surface snow scheme. The divergence of the ECHAM5-

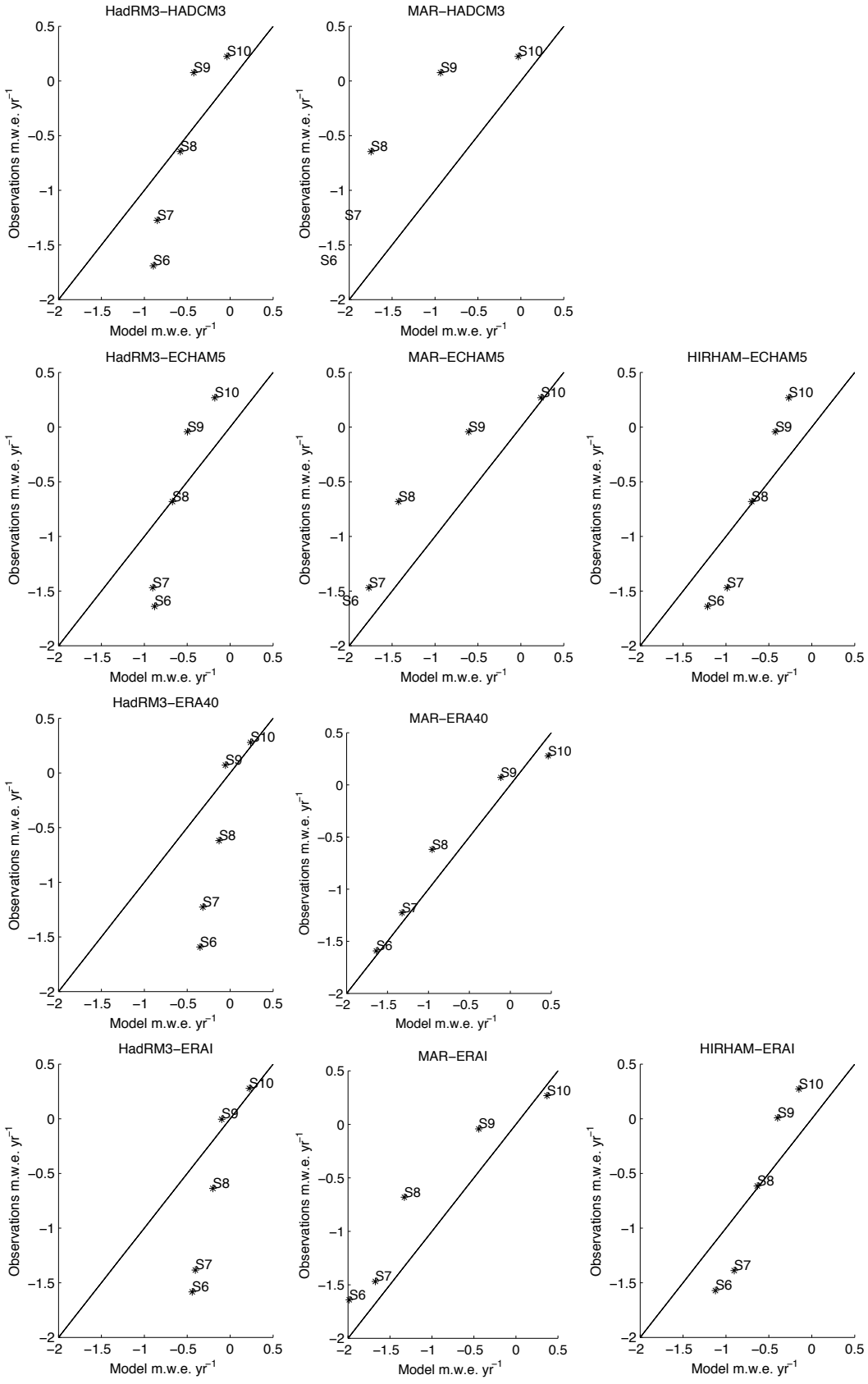

Figure 13: Simulated and observed SMB averaged over periods where data is available

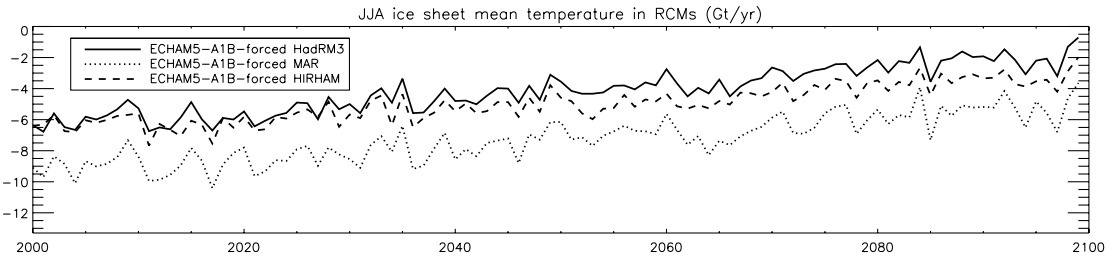

Figure 14: Time series of GrIS mean summer (JJA) $T_{\rm as}$ for the 3 RCMs, forced by ECHAM5 A1B boundary conditions

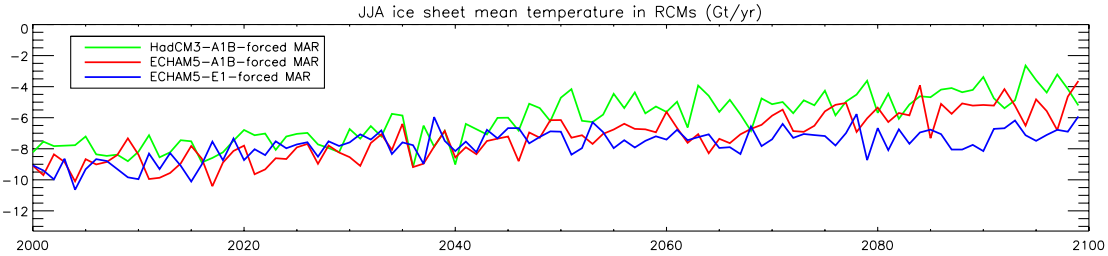

Figure 15: Time series of GrIS mean summer (JJA) $T_{\rm as}$ for MAR, forced by all 3 sets of future boundary conditions

A1B- and ECHAM5-E1-forced simulations becomes apparent later in the 21st century, implying a committment to Greenland melt up to ∼2050.

In Table 10, the following statistics are shown for GrIS mean $T_{\rm as}$ in each future simulation: anomaly of 2080-2099 mean relative to 1989-2008 mean from ERA-INTERIM-forced simulation; trend and standard error in trend for 2000-2099; and standard deviation on detrended mean for 2000-2099 (which gives an indication of the interannual variability). In all simulations, the trends were different from zero at the 2σ confidence level (denoted by the trend appearing in bold in the table). The trend is seen to be less in the simulations forced by scenario E1, due to the lower radiative forcing; this is also seen in the 2080-2099 mean anomaly relative to the appropriate ERA-INTERIM-forced simulation, also shown in the table. The improved snow scheme in MAR compared with HadRM3 and HIRHAM5 leads to an increased interannual variability (seen in the standard deviation), but not a greater sensitivity to climate change (seen in the trend). HIRHAM5, with a low albedo, is the most sensitive to climate change. Fig. 16 shows maps of 1989-2008 mean $T_{\rm as}$ over the GrIS in the ERA-INTERIM-forced simulations, and the $T_{\rm as}$ anomalies of the HadCM3-A1B, ECHAM5-A1B and ECHAM5-E1- forced simulations (2080-2099 means) relative to the ERA-INTERIM-forced simulations (1989-2008 means). In all simulations, $T_{\rm as}$ is seen to increase almost everywhere, but the increase is greater in the north. Again, it can be seen that the increase is smaller in the ECHAM-E1-forced simulations than in the A1B-forced simulations. Each RCM has its own pattern of warming in response to the different forcings (HadCM3 and ECHAM5), but in general the greatest warming

Table 10: Summer (JJA) GrIS mean $T_{\rm as}$ in future RCM runs: Anomalies of 2080-2099 means relative to 1989-2008 mean from the ERA-INTERIM-forced simulation of the appropriate model, 2000-2099 trends, and 2000-2099 standard deviations (detrended)

Forcing	RCM	2080-2099 mean, minus 1989-2008 ERA-INT-forced mean (°C)	2000-2099 trend (°C yr^{-1})	2000-2099 Std. dev. (°C)
HadCM3 A1B	HadRM3	5.5	**0.05±0.002**	2.4
	MAR	4.6	**0.05±0.003**	3.4
ECHAM5 A1B	HadRM3	5.0	**0.05±0.002**	2.6
	MAR	3.7	**0.04±0.003**	3.8
	HIRHAM5	3.0	**0.04±0.002**	2.7
ECHAM5 E1	HadRM3	3.4	**0.03±0.002**	2.6
	MAR	1.9	**0.02±0.003**	3.7
	HIRHAM5	1.5	**0.02±0.002**	2.6

is in the north.

4.2 Melt Area Extent

Fig. 17 shows scatter plots relating length of the melting season (calculated using the same algorithm as in Section 3.3, also used for calculating melt season length from satellite observations) to total summer meltwater production for HadRM3, MAR and HIRHAM5 forced by ERA-INTERIM, historical ECHAM5, and ECHAM5 A1B boundary conditions. In MAR, due to the difference between the albedo of bare ice (0.4) and that of melting snow (0.6 to 0.7), the melt is enhanced in the ablation zone when bare ice appears. The meltwater production in MAR therefore depends strongly on whether the melting gridbox is covered by melting snow or by bare ice.

As shown by *Fettweis et al.* (2011), the satellite data, and therefore the algorithm used here, is sensitive to a production of daily meltwater greater than 8 mmWE day^{-1}, but does not distinguish between gridboxes with different amounts of melt, or melting snow (where daily meltwater production is in the range 0 to 10 mmWE day^{-1}) and melting bare ice (where daily meltwater production is in the range 30 to 50 mmWE day^{-1}). Over snow, the meltwater amount is a function of the melt season length, i.e. snow melts at a low rate. For bare ice, the meltwater production is much higher, but this does not increase the satellite's melt season length. Thus, once a gridbox becomes bare ice, the relationship between melt season length and meltwater production breaks down.

Finally, it can be seen from Fig. 17 that the relationship between length of melting season and total meltwater production is the same in the future (ECHAM5-A1B) scenario as in the historical simulations. Thus, these results indicate that the current ratio of melting season length to meltwater production is likely to be conserved in warmer climates. The only difference in a warmer climate is that there is an increase in the number of gridboxes with a longer melt season, and there is therefore a corresponding increase in meltwater production.

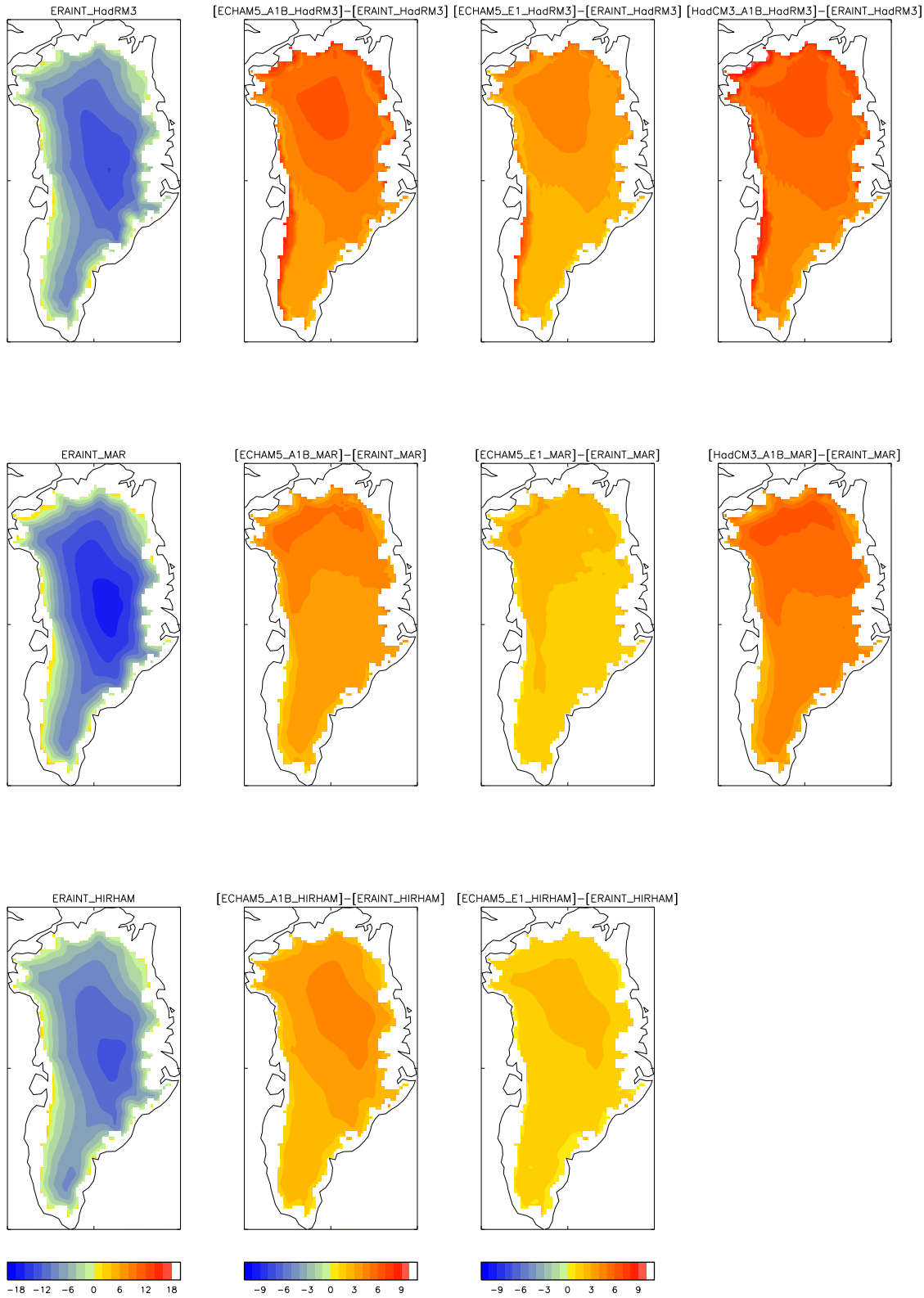

Figure 16: T_{as} over the GrIS. Top row: HadRM3; middle row: MAR; bottom row: HIRHAM5. Columns from left: 1989-2008 means from ERA-INTERIM-forced simulations; and 2080-2099 mean anomalies of ECHAM5-A1B-, ECHAM5-E1- and HadCM3-A1B-forced simulations, relative to 1989-2008 means from ERA-INTERIM-forced simulations.

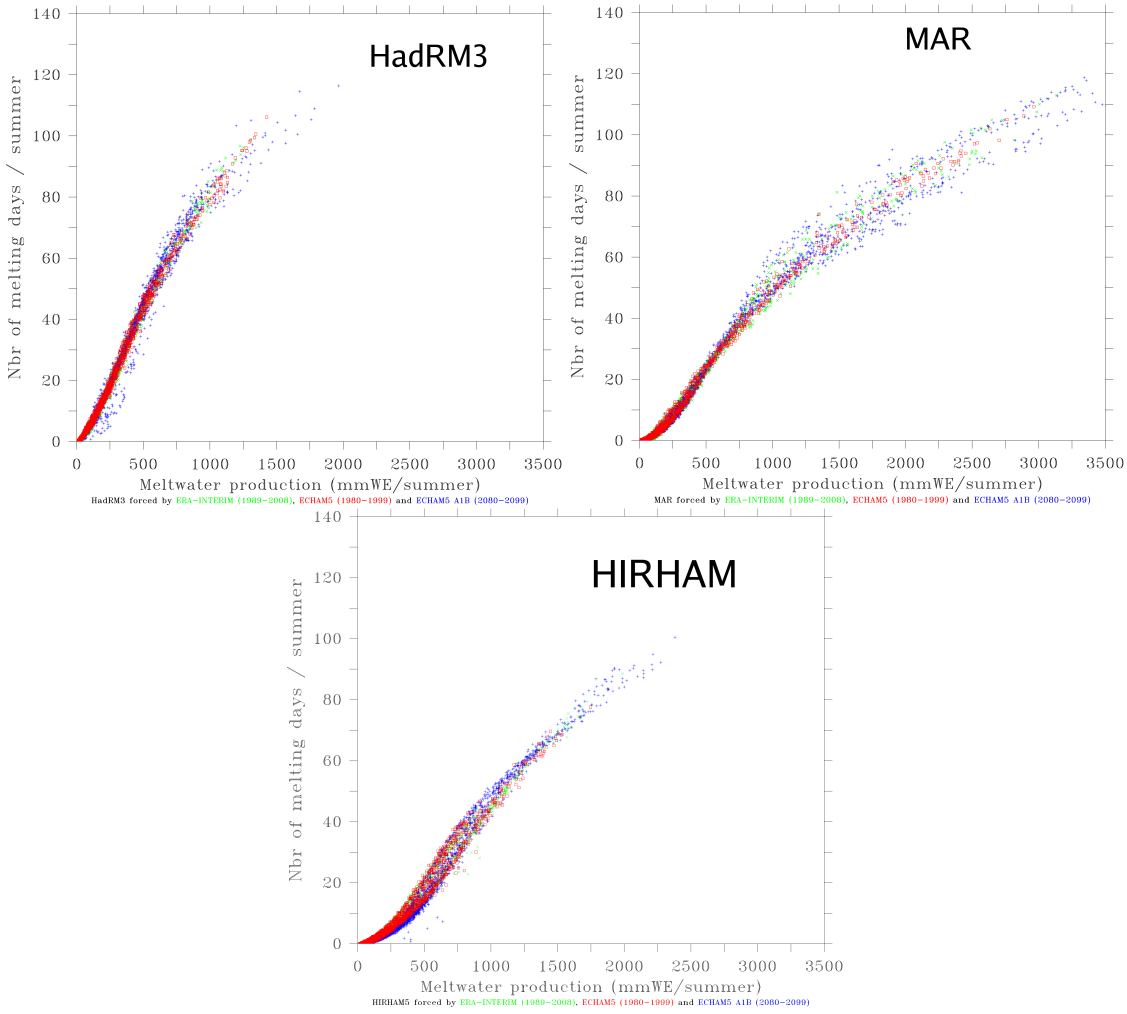

Figure 17: Scatter plot of the mean number of melt days versus the mean annual meltwater production (in mmWE yr^{-1}) simulated by the 3 RCMs forced by ERA-INTERIM over 1989-2008, ECHAM5 over 1980-1999 and ECHAM5 over 2080-2099.

4.3 Components of surface mass balance

Time series for snowfall, melt, refreezing and runoff for the ECHAM5-A1B-forced simulations of all 3 RCMs are shown in Fig. 18. Total snowfall is similar in HadRM3 and MAR, but higher in HIRHAM5. This may be because the domain used in the HIRHAM5 simulations is larger than that used in the other 2 models, leading to more water vapour being picked up locally. Melt, on the other hand, is similar in MAR and HIRHAM5, but lower in HadRM3, presumably because of its higher albedo, as discussed in Section 3.3. HadRM3 and MAR give similar refreezing, possibly because the offline refreezing scheme used for HadRM3 was tuned so that it gave similar results to MAR in the historical period. HIRHAM5 does not calculate refreezing. Because HadRM3 has less melt than MAR, but they both have similar refreezing, the runoff from HadRM3 is less than that from MAR. Similarly, because MAR and HIRHAM5 produce similar melt, but only HIRHAM5 includes refreezing, the runoff from MAR is less than that from HIRHAM5.

Again, the sensitivity of an individual RCM to choice of boundary conditions is studied by plotting time series for the 3 MAR simulations in Fig. 19. Snowfall in MAR is seen to be largely insensitive to the choice of boundary conditions. Melt is greater in the two A1B-forced simulations than in the E1-forced simulation, because of the lower temperatures, and lower radiative forcing, in the latter. Refreezing is similar in the ECHAM5-A1B- and ECHAM5-E1-forced simulations, but greater in the HadCM3-A1B-forced simulation. Runoff is greater in the ECHAM5-A1B-forced simulation than in the ECHAM5-E1-forced simulation, because the former has greater melt and they have similar refreezing. The HadCM3-A1B-forced simulation gives less runoff than the corresponding ECHAM5-forced simulation because the former has more refreezing.

In Table 11, the following statistics are shown for GrIS total snowfall, melt, refreezing and runoff in each future simulation: anomaly of 2080-2099 mean relative to 1989-2008 mean from ERA-INTERIM-forced simulation; trend and standard error in trend for 2000-2099; and standard deviation on detrended mean for 2000-2099. The trend in snowfall is seen to be significant at the 2σ level for both HadCM3-A1B-forced simulations, and for the ECHAM5-A1B-forced simulations from MAR and HIRHAM5. It is not significant at this level for any of the ECHAM5-E1-forced simulations. The trend in melt is significant at the 2σ level in all simulations. It is always smaller in the ECHAM5-E1-forced simulations than in the equivalent A1B-forced simulations, due to the lower radiative forcing in that scenario. The trends in MAR are always greater than those in HadRM3 and HIRHAM5. The refreezing is greater than the standard deviation in all A1B-forced simulations of HadRM3 and MAR, and in the ECHAM5-E1-forced HadRM3 simulation (where it was calculated offline), but not in the equivalent MAR simulation. The trends in runoff are siginificant at the 2σ level in all simulations except ECHAM5-E1-forced HadRM3, despite the trend in melt being significant in this simulation. However, the trend in melt, although just inside the 2σ confidence limit, is relatively small; this, combined with the effect of refreezing, has probably led to the lack of a significant trend in runoff.

Figs. 20 to 22 show maps of 1989-2008 mean snowfall, melt and refreezing in the ERA-INTERIM-

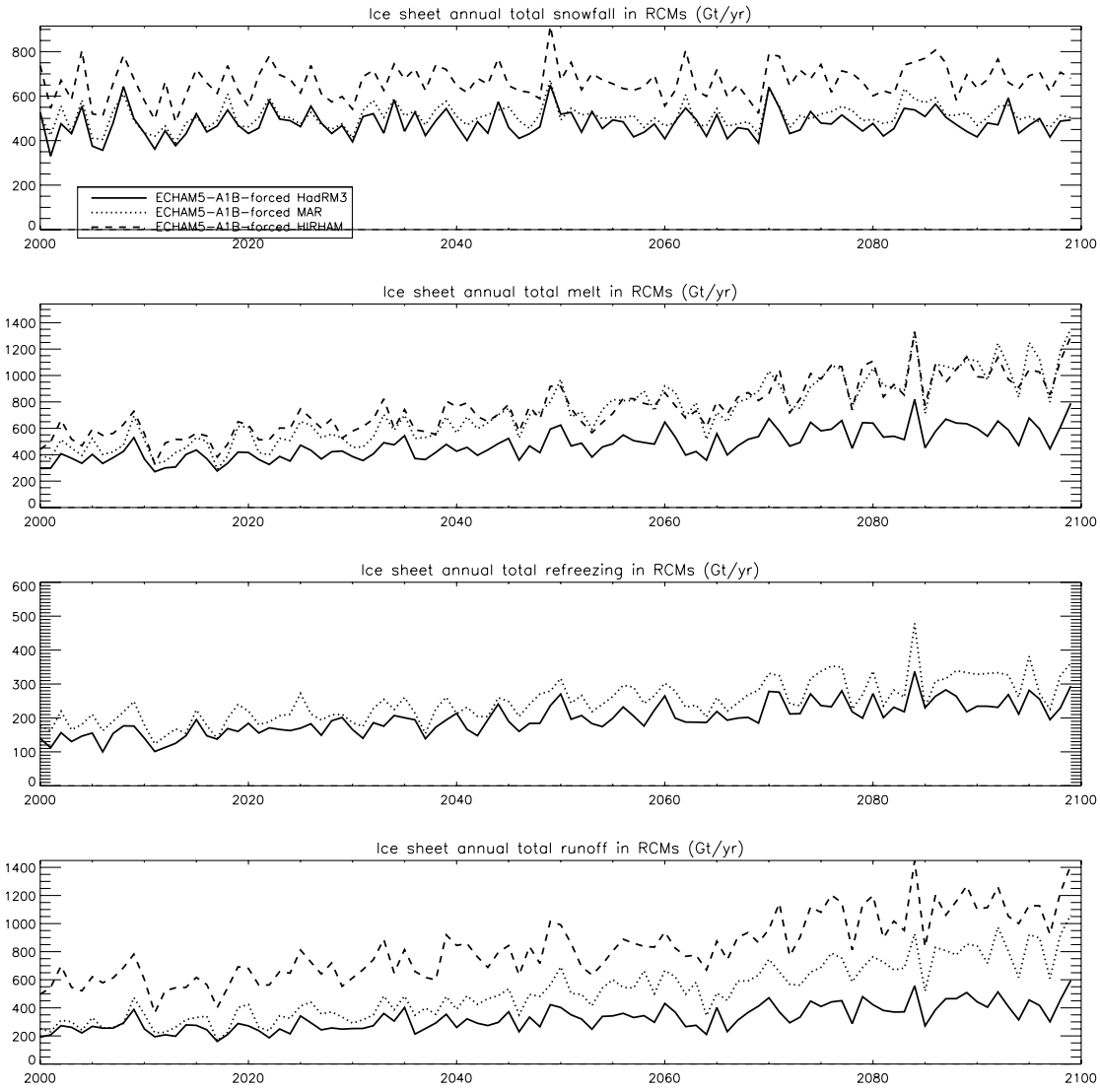

Figure 18: Time series of GrIS total snowfall, melt, refreezing and runoff for the 3 RCMs, forced by ECHAM5 A1B boundary conditions. Note that there is no representation of refreezing in HIRHAM5. The HadRM3 rerfreezing was calculated offline.

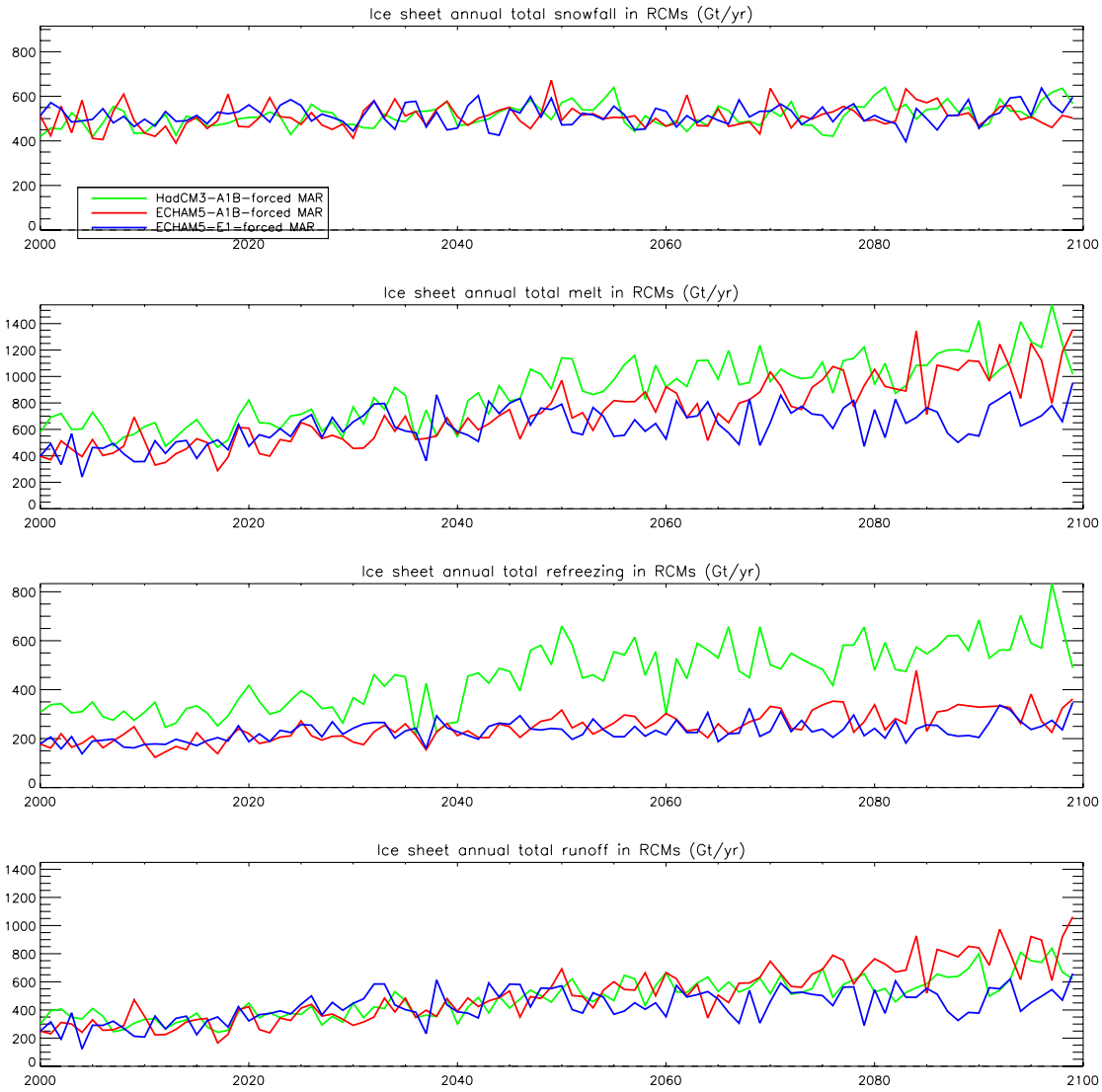

Figure 19: Time series of GrIS total snowfall, melt, refreezing and runoff for MAR, forced by all 3 sets of future boundary conditions.

Table 11: Snowfall, melt, refreezing and runoff in the future RCM simulations. 2080-2099 means, expressed as anomalies relative to 1989-2008 means from ERA-INTERIM-forced simulations; 2000-2099 trends; and 2000-2099 standard deviations (detrended) Trends which are different from zero at the 2σ confidence level are shown in bold.

Forcing	RCM	Snowfall			Melt			Refreezing			Runoff		
		2080 -2099 mean anomaly (Gt yr^{-1})	2000 -2099 trend (Gt yr^{-2})	2000 -2099 Std. dev. (Gt yr^{-1})	2080 -2099 mean anomaly (Gt yr^{-1})	2000 -2099 trend (Gt yr^{-2})	2000 -2099 Std. dev. (Gt yr^{-1})	2080 -2099 mean anomaly (Gt yr^{-1})	2000 -2099 trend (Gt yr^{-2})	2000 -2099 Std. dev. (Gt yr^{-1})	2080 -2099 mean anomaly (Gt yr^{-1})	2000 -2099 trend (Gt yr^{-2})	2000 -2099 Std. dev. (Gt yr^{-1})
HadCM3 A1B	HadRM3	-47	**+0.43±0.21**	206	380	**+3.05±0.27**	160	134	**+1.35±0.11**	65	317	**+2.38±0.27**	109
	MAR	-34	**+0.74±0.16**	189	719	**+7.24±0.44**	217	379	**+3.63±0.27**	111	387	**+4.06±0.25**	118
ECHAM5 A1B	HadRM3	-117	+0.24±0.21	186	327	**+2.96±0.26**	137	96	**+1.26±0.10**	54	282	**+2.26±0.22**	93
	MAR	-66	**+0.37±0.18**	195	622	**+7.48±0.41**	159	107	**+1.60±0.14**	69	547	**+6.27±0.32**	98
	HIRHAM5	-131	**+0.54±0.26**	256	446	**+5.94±0.39**	197	N/A	N/A	N/A	497	**+6.62±0.43**	210
ECHAM5 E1	HadRM3	-99	+0.12±0.18	198	148	**+0.54±0.26**	144	60	**+0.73±0.08**	57	120	+0.06±0.23	98
	MAR	-63	+0.20±0.16	203	269	**+2.80±0.41**	174	45	**+0.72±0.12**	72	241	**+2.22±0.32**	111
	HIRHAM5	-139	+0.14±0.22	268	141	**+1.56±0.40**	229	N/A	N/A	N/A	161	**+1.78±0.43**	247

forced simulations, and the anomalies in these quantities from the HadCM3-A1B, ECHAM5-A1B and ECHAM5-E1-forced simulations (2080-2099 means) relative to the ERA-INTERIM-forced simulations (1989-2008 means). From Fig. 20, it can be seen that in all simulations the snowfall increases in some regions and decreases in others, leading to the lack of a trend seen for all simulations in Table 11. In Fig. 21, it can be seen that there are large increases in melt in the ablation zone in MAR, while the increases are smaller in HadRM3 and MAR. This leads to the differences in trends in melt between the models seen in Table 11, where MAR has much larger trends in all simulations than the equivalent simulations with the other 2 models. The E1-forced simulations all have smaller increases in melt than the equivalent A1B-forced simulations. Finally, the changes in refreezing (Fig. 22) in the ablation zone are small compared to the increases in melt. The large difference in refreezing between MAR simulations forced by ECHAM5 and the simulation forced by HadCM3, seen in Fig. 19, is also seen in the bottom row of Fig. 22, where it appears to occur throughout the ablation zone.

4.4 Surface Mass Balance

Fig. 23 shows time series of SMB for the ECHAM5-A1B-forced simulations for all 3 RCMs. MAR and HIRHAM5 both give noticeable downward trends, with the SMB becoming negative around the mid-21st century. The SMB from HadRM3, on the other hand, while having a significant downward trend (see the last 2 columns of Table 12), never becomes negative. Fig. 24 shows the sensitivity of the MAR output to choice of boundary conditions. There is a downward trend for all 3 simulations, which is more pronounced in the two A1B-forced runs.

In Table 12, the following statistics are shown for GrIS mean SMB in each future simulation: anomaly of 2080-2099 mean relative to 1989-2008 mean from ERA-INTERIM-forced simulation; trend and standard error in trend for 2000-2099; and standard deviation on detrended mean for 2000-2099. The trends in SMB are seen to be significant at the 2σ level in all simulations except ECHAM5-E1-forced HadRM3. That simulation lacks a significant trend probably because of the lack of significant trends in both snowfall and runoff. As already discussed, the latter was probably caused by a combination of a relatively-small trend in melt, and the presence of refreezing.

Fig. 25 shows maps of 1989-2008 mean SMB in the ERA-INTERIM-forced simulations, and the anomalies in these quantities from the HadCM3-A1B, ECHAM5-A1B and ECHAM5-E1-forced simulations (2080-2099 means) relative to the ERA-INTERIM-forced simulations (1989-2008 means). The decrease in melt seen in the west for HadRM3 in Fig. 21 leads to a co-located increase in SMB in Fig. 25. Elsewhere in the ablation zone for HadRM3 there is a decrease because of increasing melt. MAR has the greatest decrease in SMB in the ablation zone because of its bare ice albedo, whereas HIRHAM5 has the smallest increase because of its widespread low albedo. However, the SMB in HIRHAM5 decreases almost everywhere, especially for the ECHAM5-A1B-forced run, including many areas well inland away from the ablation zone. This feature does not occur to such a

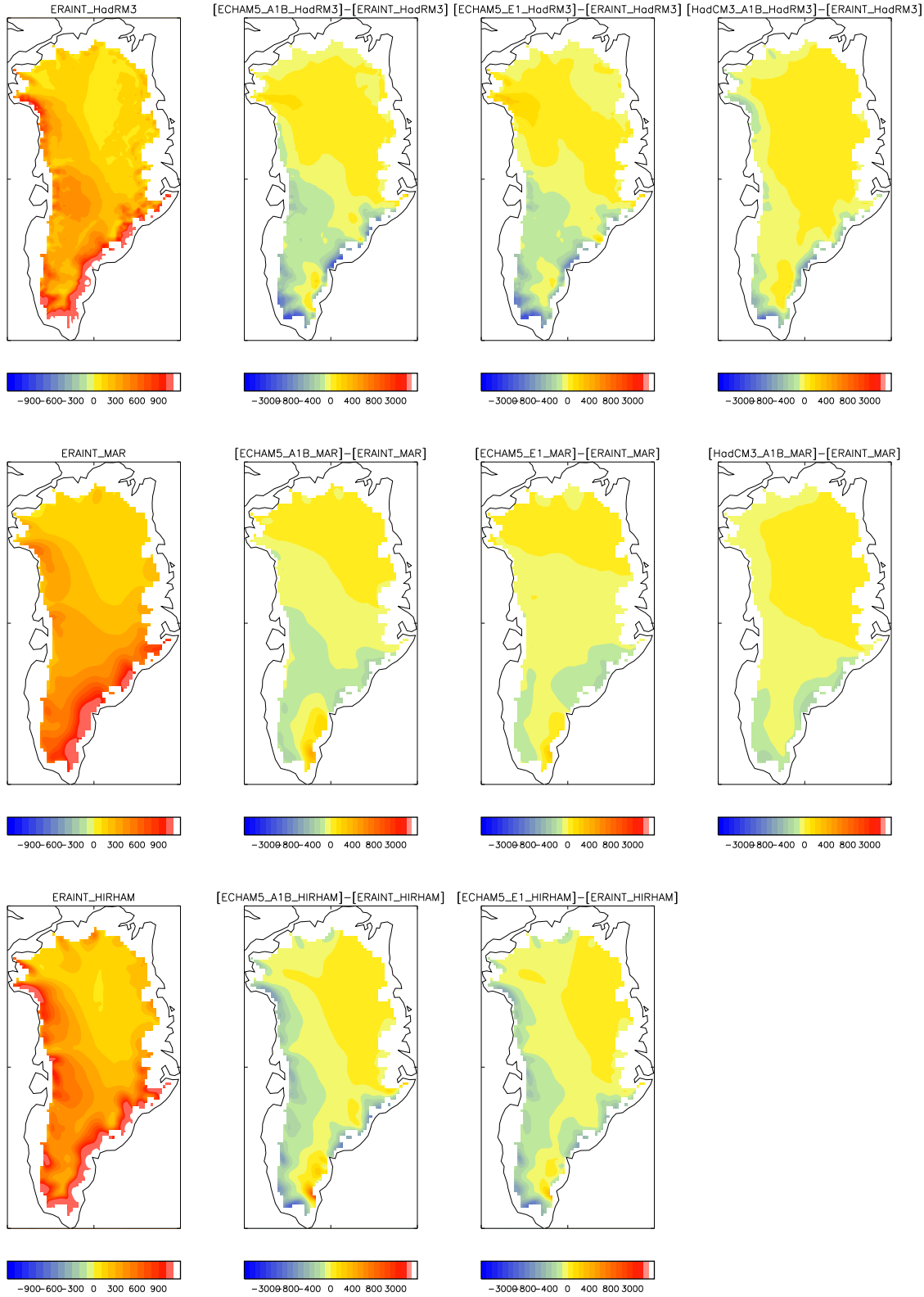

Figure 20: Snowfall over the GrIS. Top row: HadRM3; middle row: MAR; bottom row: HIRHAM5. Columns from left: 1989-2008 means from ERA-INTERIM-forced simulations; and 2080-2099 mean anomalies of ECHAM5-A1B-, ECHAM5-E1- and HadCM3-A1B-forced simulations, relative to 1989-2008 means from ERA-INTERIM-forced simulations.

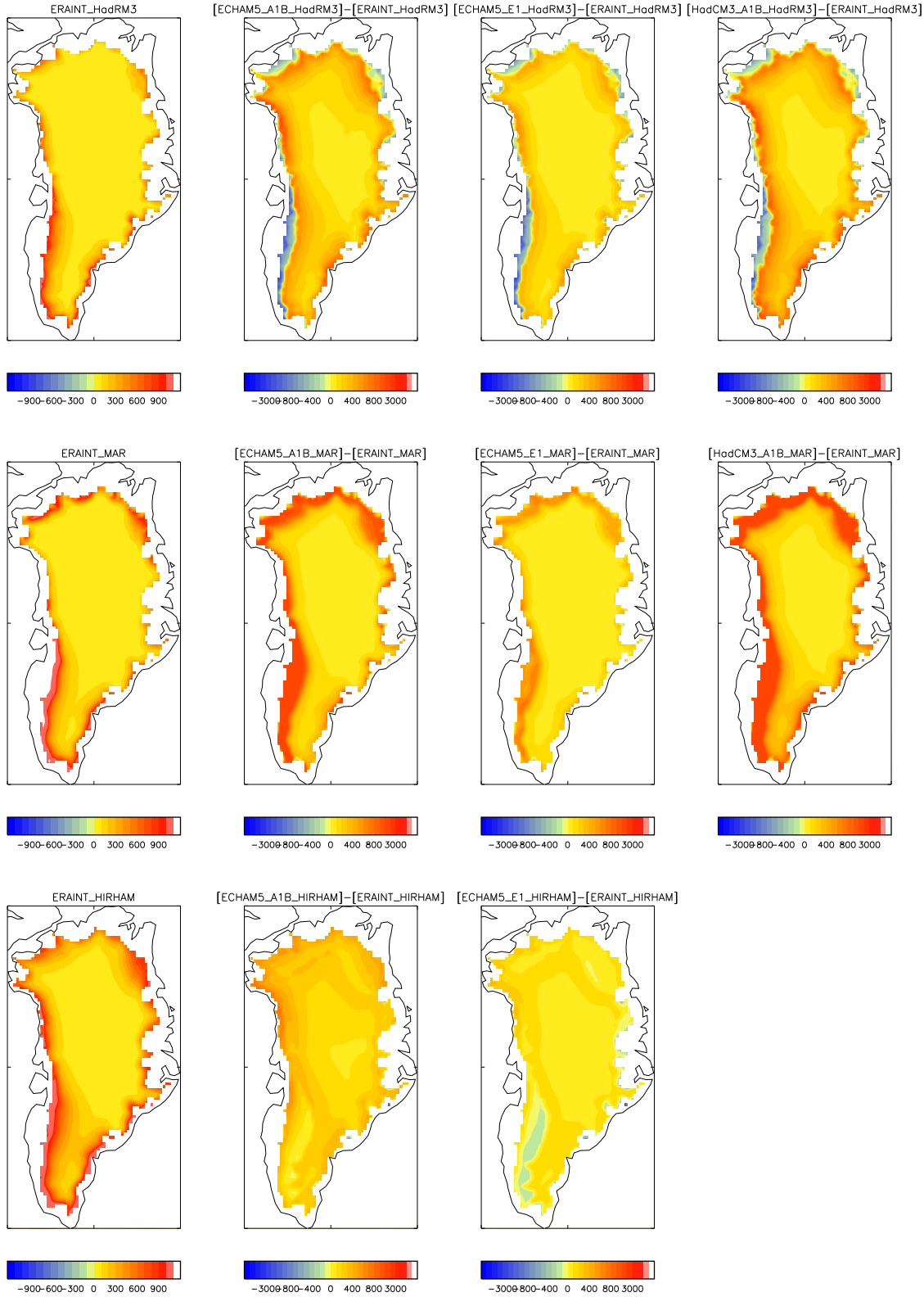

Figure 21: Snow melt over the GrIS. Top row: HadRM3; middle row: MAR; bottom row: HIRHAM5. Columns from left: 1989-2008 means from ERA-INTERIM-forced simulations; and 2080-2099 mean anomalies of ECHAM5-A1B-, ECHAM5-E1- and HadCM3-A1B-forced simulations, relative to 1989-2008 means from ERA-INTERIM-forced simulations.

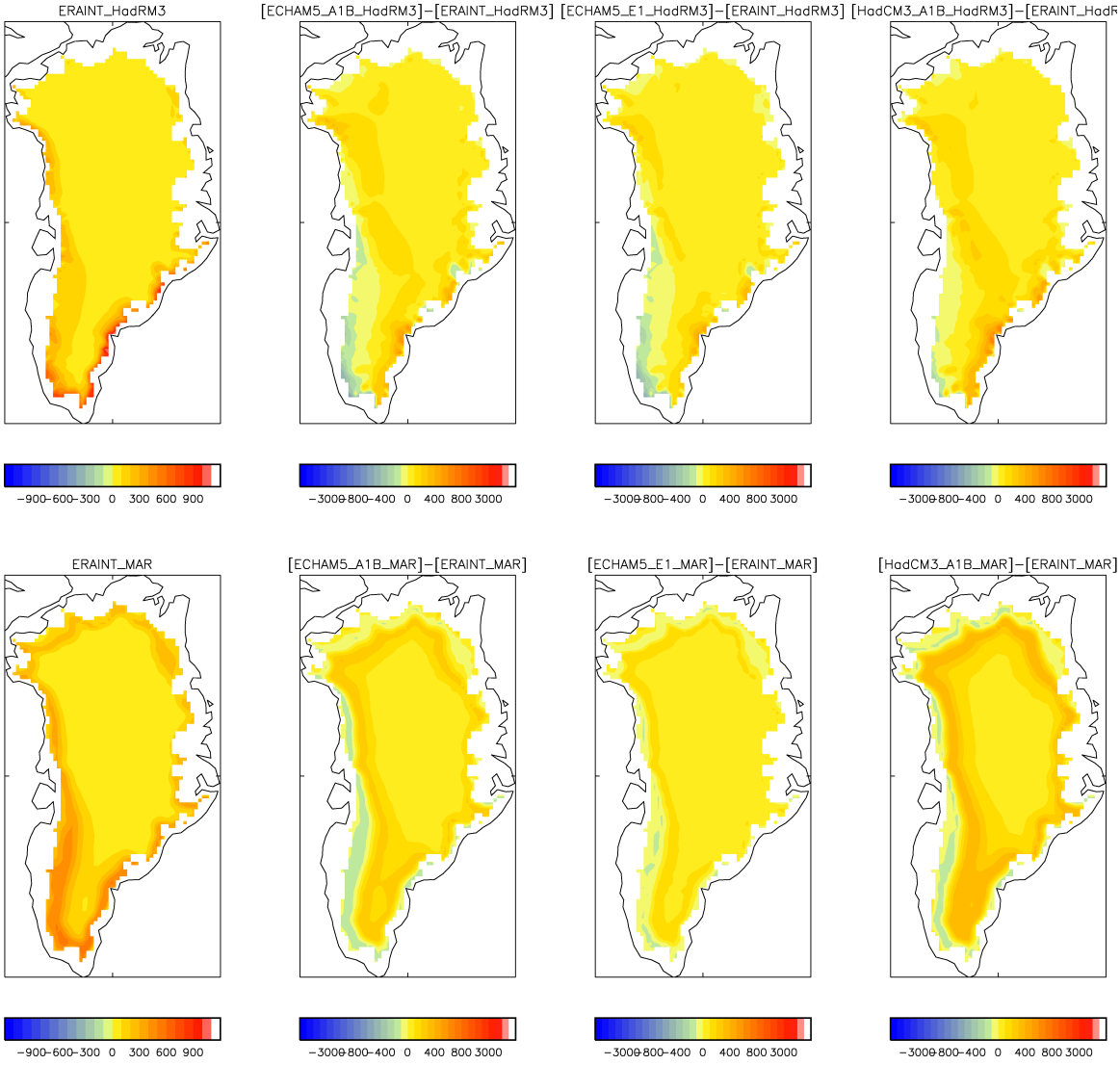

Figure 22: Refreezing of meltwater. Top row: HadRM3; bottom row: MAR. Columns from left: 1989-2008 means from ERA-INTERIM-forced simulations; and 2080-2099 mean anomalies of ECHAM5-A1B-, ECHAM5-E1- and HadCM3-A1B-forced simulations, relative to 1989-2008 means from ERA-INTERIM-forced simulations.

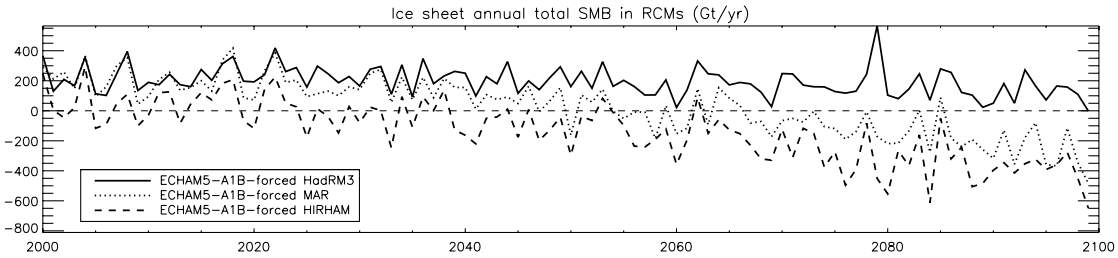

Figure 23: Time series of GrIS total annual mass balance for the 3 RCMs, forced by ECHAM5 A1B boundary conditions

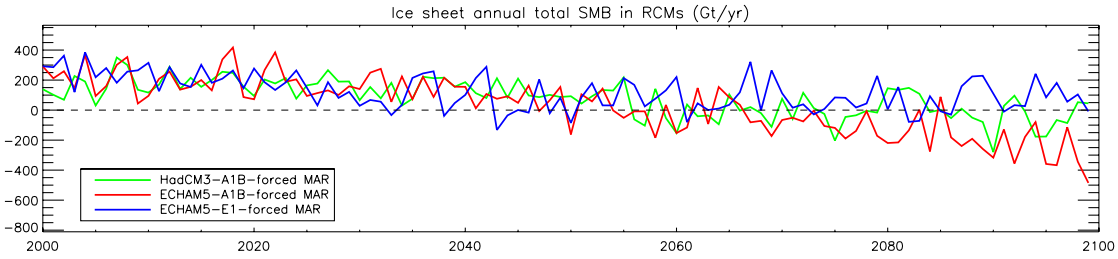

Figure 24: Time series of GrIS total annual mass balance for MAR, forced by all 3 sets of future boundary conditions

Table 12: GrIS total SMB in future RCM runs: Anomalies of 2080-2099 means relative to 1989-2008 mean from the ERA-INTERIM-forced simulation of the appropriate model, 2000-2099 trends, and 2000-2099 standard deviations (detrended)

Forcing	RCM	2080-2099 mean, minus 1989-2008 ERA-INT-forced mean (Gt yr^{-1})	2000-2099 trend (Gt yr^{-2})	2000-2099 Std. dev. (Gt yr^{-1})
HadCM3 A1B	HadRM3	-269	**-1.10±0.36**	117
	MAR	-369	**-2.81±0.31**	92
ECHAM5 A1B	HadRM3	-335	**-1.33±0.28**	103
	MAR	-576	**-5.47±0.36**	116
	HIRHAM5	-564	**-5.34±0.44**	69
ECHAM5 E1	HadRM3	-180	+0.37±0.29	112
	MAR	-284	**-1.87±0.36**	108
	HIRHAM5	-268	**-1.37±0.44**	48

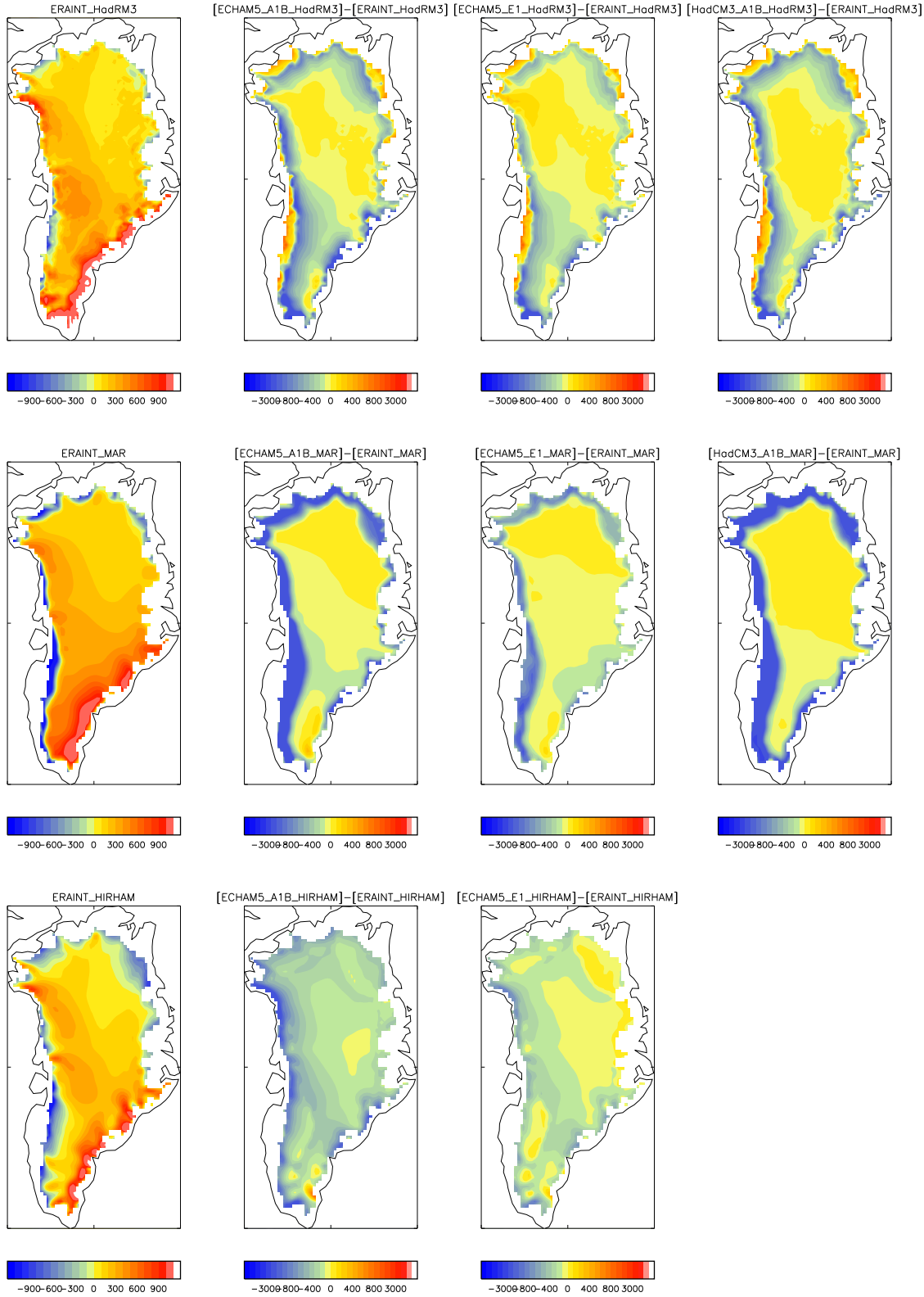

Figure 25: Surface mass balance. Top row: HadRM3; middle row: MAR; bottom row: HIRHAM5. Columns from left: 1989-2008 means from ERA-INTERIM-forced simulations; and 2080-2099 mean anomalies of ECHAM5-A1B-, ECHAM5-E1- and HadCM3-A1B-forced simulations, relative to 1989-2008 means from ERA-INTERIM-forced simulations.

great extent in HadRM3, so that in Table 12 the anomaly and trend in total SMB in that model are smaller than in MAR and HIRHAM5.

5 Summary and conclusions

Four Regional Climate Models (RCMs) - HadRM3, MAR, HIRHAM5 and RACMO2 - have been run for Greenland to produce results for the recent past, forced at the domain boundaries by reanalysis data as well as output from 2 General Circulation Models (GCMs). Three of these RCMs - HadRM3, MAR and HIRHAM5 - were also run to produce results for future scenarios for the 21$^{\rm st}$ century. The historical output has been validated against available observations of surface air temperature, accumulation, meltwater amount, melt area extent and surface mass balance.

The model evaluation reveals that for surface air temperatures ($T_{\rm as}$), RACMO2 gave the best agreement with observations and HadRM3 the worst. HadRM3 consistently simulates low $T_{\rm as}$ at stations near the coast. HadRM3 and HIRHAM5 both overestimate melt area extent relative to satellite observations at the start of the melt season and underestimate it at the end. This could be attributable to the snow albedo representation in these models, or to the lack of adequate snow physics schemes. 20-year mean surface mass balance (SMB) in the simulations of the recent past was in the range 30 – 469 Gt yr^{-1}. The SMB in simulations forced by GCM output was generally smaller than those forced by reanalysis data, because there is less precipitation in the GCM-forced simulations. Interannual variability in SMB was found to depend more on the forcing rather than specific RCMs, whereas mean SMB depended on both RCM and forcing. Evaluation of SMB against some of the few available in-situ observations shows that overall MAR gave the best simulation of SMB, and HadRM3 the worst; however, this was not an extensive analysis.

Trends in Greenland ice sheet mean $T_{\rm as}$ during the 21$^{\rm st}$ century are $\sim$0.04 – 0.05°C yr^{-1} for the SRES A1B scenario, and $\sim$0.02 – 0.03°C yr^{-1} for the E1 mitigation scenario (all significant at the 2σ level). Trends in SMB were $\sim$-5.5 – -1.1 Gt yr^{-2} for the A1B scenario (all significant at the 2σ level). In the 2 E1-forced simulations where the SMB trend was significant at the 2σ level, the trends were -1.9 and -1.4 Gt yr^{-2}. SMB trends were dominated by trends in melt rather than trends in precipitation.

Overall, the models with multi-layer snow schemes (MAR and RACMO2) give better agreement with observations than the other 2 models (HadRM3 and HIRHAM5). We have shown that, with a detailed snow scheme, RCMs at high resolution represent an improvement over coarser-resolution GCMs. However, we have also shown the importance of such a snow scheme for SMB. Some coarse-resolution GCMs apparently give reasonably-accurate results for SMB (e.g. *Ridley et al.*, 2005); however, this is because the underestimation of melt is compensated for by the lack of refreezing. When the same surface scheme is run in a high-resolution RCM, the melt is calculated more accurately, so that the lack of refreezing leads to the SMB being underestimated. Here, for HadRM3, we have solved this by calculating refreezing offline, but for future work it is essential that

a multi-layer snow scheme that includes meltwater percolation, retention and refreezing is used.

Calculation of the total mass balance (rather than SMB) would require a simulation of ice dynamics, ice shelves, and fast-flowing ice streams. In order to make projections into the future, ice sheet models require accurate forcing by the atmosphere and ocean. We recommend the development of coupled atmosphere-ice sheet-ocean model systems that can simulate the response of the Greenland and Antarctic Ice Sheets to rising temperatures and calculate the freshwater flux that can be expected to the ocean. It is to be hoped that future work on developing a new generation of Earth System Models (ESMs) will resolve some of the deficiencies in current RCM simulations of ice sheet climate and mass balance for both Greenland and Antarctica.

References

Bales, R.C., Q. Guo, D. Shen, J.R. McConnell, G. Du, J.F. Burkhart, V.B. Spikes, E. Hanna, and J. Cappelen (2009), Annual accumulation for Greenland updated using ice core data developed during 2000-2006 and analysis of daily coastal meteorological data, *J.Geophys.Res.*, *114*, D06116, doi:10.1029/2008JD011208.

Bamber, J.L., S. Ekholm and W.B. Krabill (2001), A new, high-resolution digital elevation model of Greenland fully validated with airborne laser altimeter data *J.Geophys.Res.*, *106*, B4, 6733-6745

Bougamont, M., J. L. Bamber, J. K. Ridley, R. M. Gladstone, W. Greuell, E. Hanna, A. J. Payne, and I. Rutt (2007), Impact of model physics on estimating the surface mass balance of the Greenland ice sheet, Geophys. Res. Lett., 34, L17501, doi:10.1029/2007GL030700.

Box, J.E., and K. Steffen (2000), *Greenland Climate Network (GC-NET) Data Reference*, University of Colorado. Available at `http://cires.colorado.edu/science/groups/steffen/gcnet/`

Box, J.E., and A. Rinke (2003), Evaluation of Greenland ice sheet surface climate in the HIRHAM Regional Climate Model using automatic weather station data, *J.Clim.*, *16*, 1302-1319.

Box, J.E., D.H. Bromwich, and L.-S. Bai (2004), Greenland ice sheet surface mass balance 1991-2000: Application of Polar MM5 mesoscale model and in situ data, *J.Geophys.Res.*, *109*, D16105, doi:10.1029/2003JD004451.

Box, J.E., D.H. Bromwich, B.A. Veenhuis, L.-S. Bai, J.C. Stroeve, J.C. Rogers, K. Steffen, T. Haran, and S.-H. Wang (2006), Greenland Ice Sheet Surface Mass Balance Variability (1988-2004) from Calibrated Polar MM5 Output, *J.Climate*, *19*, 2783-2800.

Brun, E., P. David., M. Sudul and G. Brunot (1992), A numerical model to simulate snowcover stratigraphy for operational avalanche forecasting, *J. Glaciol.*, *38*, 13-22.

Cappelen, J., B.V. Jorgensen, E.V. Laursen, L.S. Stannius, and R.S. Thomsen (2000) *The Observed Climate of Greenland, 1958-99 - with Climatological Standard Normals, 1961-90* DMI Technical Report 00-18, DMI, Copenhagen, Denmark. Available at `http://www.dmi.dk/dmi/index/viden/dmi-publikationer/tekniskerapporter/`.

Cappelen, J. (ed) (2011), *DMI Monthly Climate Data Collection 1768-2010, Denmark, The Faroe Islands and Greenland*, DMI Technical Report 11-05, DMI, Copenhagen, Denmark. Available at `http://www.dmi.dk/dmi/index/viden/dmi-publikationer/tekniskerapporter/`.

Cogley, J.G. (2004), Greenland accumulation: An error model, *Journal of Geophysical Research*, *109*, D18101, doi:10.1029/2003JD004449.

Dethloff, K., M. Schwager, J.H. Christensen, S. Kiilsholm, A. Rinke, W. Dorn, F. Jung-Rothenhäusler H. Fischer, S. Kipfstuhl, and H. Miller (2002), Recent Greenland accumulation estimated from Regional Climate model simulations and ice core analysis, *J.Clim.*, *15*, 2821-2832.

Eerola, K. (2006), *About the performance of HIRLAM version 7.9*, HIRLAM Newsletter No. 51 Article 14, available at `http://hirlam.org`

Essery R., M. Best and P. Cox (2001), *MOSES 2.2 Technical Documentation*, Hadley Centre Technical Note 30, Met Office Hadley Centre, Bracknell, UK, 30pp

Ettema, J. (2010), *The present-day climate of Greenland; A study with a regional climate model*, PhD thesis, Utrecht University.

Ettema, J., M. R. van den Broeke, E. van Meijgaard, W. J. van de Berg, J. L. Bamber, J. E. Box and R. C. Bales (2009), Higher surface mass balance of the Greenland ice sheet revealed by high-resolution climate modelling, *Geophys.Res.Lett.*, *36*, L12501.

Ettema, J., M. R. van den Broeke, E. van Meijgaard, W. J. van de Berg, J. E. Box and K. Steffen (2010), Climate of the Greenland ice sheet using a high-resolution climate model, Part 1: Evaluation, *The Cryosphere*, *4*, 511-527.

Fettweis, X., H. Gallée, F. Lefebre, and J.-P. van Ypersele (2005), Greenland surface mass balance simulated by a regional climate model and comparison with satellite-derived data in 1990-1991, *Clim.Dyn.*, *24*, 623-640.

Fettweis, X., E. Hanna, H. Gallée, P. Huybrechts, and M. Erpicum (2008), Estimation of the Greenland ice sheet surface mass balance for the 20^{th} and 21^{st} centuries, *The Cryosphere*, *2*, 117-129.

Fettweis, X., M. Tedesco, M. van den Broeke and J. Ettema (2011), Melting trends over the Greenland ice sheet (1958-2009) from spaceborne microwave data and regional climate models, *The Cryosphere*, *5*, 359-375, doi:10.5194/tc-5-359-2011.

Gallée, H., G. Guyomarc'h and E. Brun (2001), Impact of the snow drift on the Antarctic ice sheet surface mass balance: possible sensitivity to snow-surface properties, *Boundary-Layer Meteorol.*, *99*, 1-19.

Gallée, H. and G. Schayes, (1994), Development of a three-dimensional meso-γprimitive equations model, *Mon. Wea. Rev.*, *122*, 671-685.

Gordon, C., C. Cooper, C.A. Senior, H. Banks, J.M. Gregory, T.C. Johns, J.F.B. Mitchell and R.A. Wood (2000), The simulation of SST, sea ice extents and ocean heat transports in a version of the Hadley Centre coupled model without flux adjustments, *Clim.Dyn.*, *16*, *2-3*, 147-168

Gregory, J.M., and P. Huybrechts (2006), Ice-sheet contributions to future sea-level change. *Phil.Trans.Roy.Soc.*, *364*, 1709-1731, doi:10.1098/rsta.2006.1796.

Hagdorn, M., I. Rutt, T. Payne, and F. Hebeler (2010), *GLIMMER 1.5.1 Documentation*, Universities of Edinburgh, Bristol and Zurich, available at `http://www.cesm.ucar.edu/models/cesm1.0/cism/docs/glimmer.pdf`.

Hanna, E., P. Huybrechts, I. Janssens, J. Cappelen, K. Steffen, and A. Stephens (2005), Runoff and mass balance of the Greenland ice sheet: 1958-2003, *J.Geophys.Res.*, *110*, D13108, doi:10.1029/2004JD005641.

Hanna, E., P. Huybrechts, K. Steffen, J. Cappelen, R. Huff, C. Shuman, T. Irvine-Fynn, S. Wise, and M. Griffiths (2008), Increased Runoff from Melt from the Greenland Ice Sheet: A Response to Global Warming, *J.Climate*, *21*, 331-341.

Huybrechts, P., A. Letreguilly, and N. Reeh (1991), The Greenland ice sheet and greenhouse warming, *Palaeogeography, Palaeoclimatology, Palaeoecology*, *89*, 399-412.

Huybrechts, P., J. Gregory, I. Janssens, and M. Wild (2004), Modelling Antarctic and Greenland volume changes during the 20th and 21st centuries forced by GCM time slice integrations, *Global Planet. Change*, *42*, 83-105.

Jones, R.G., M. Noguer, D.C. Hassell, D. Hudson, S.S. Wilson, G.J. Jenkins and J.F.B. Mitchell (2004), *Generating high resolution climate change scenarios using PRECIS*, Met Office Hadley Centre, Exeter, UK, 40pp

Kiilsholm, S., J.H. Christensen, K. Dethloff, and A. Rinke (2004), Net accumulation of the Greenland ice sheet: High resolution modeling of climate changes, *Geophys.Res.Lett.*, *30*, 9, 1485, doi:10.1029/2002GL015742.

Lefebre, F., X. Fettweis, H. Gallée, J.-P. van Ypersele, P. Marbaix, W. Greuell, and P. Calanca (2005), Evaluation of a high-resolution regional climate simulation over Greenland, *Clim.Dyn.*, *25*, 99-116, doi:10.1007/s00382-005-0005-8.

Letreguilly, A., P. Huybrechts, and N. Reeh (1991a), Steady-state characteristics of the Greenland ice-sheet under different climates, *J.Glaciol.*, *37*, 149-157.

Letreguilly, A., N. Reeh, and P. Huybrechts (1991b), The Greenland ice-sheet through the last glacial-interglacial cycle, *Palaeogeography, Palaeoclimatology, Palaeoecology*, *90*, 385-394.

Lowe, J.A., C.D. Hewitt., D.P. van Vuuren, T.C. Johns, E. Stehfest, J.F. Royer, and P. van der Linden (2009), *New study for climate modelling, analyses, and scenarios*, EOS Trans AGU 90:181-182.

Lucas-Picher, P., M. Wulff-Nielsen, J.H. Christensen, G. Aðalgeirsdóttir, R. Mottram, and S.B. Simonsen (2011), Very high resolution regional climate model simulations over Greenland - identifying added value, accepted by *J.Geophys.Res.*

Marshall, S.E. (1989), *A physical parameterization of snow albedo for use in climate models*, NCAR Co-operative Thesis 123, National Center for Atmospheric Research, Boulder, Colorado, USA.

Meehl, G.A., W.D. Collins, P. Friedlingstein, A.T. Gaye, J.M. Gregory, A. Kitoh, R. Knutti, J.M. Murphy, A. Noda, S.C.B. Raper, I.G. Watterson, A.J. Weaver, and Z.-C. Zhao (2007), Global Climate Projections, In: *Climate Change 2007: The Physical Science Basis. Contribution of Working Group I to the Fourth Assessment Report of the Intergovernmental Panel on Climate Change* [Solomon, S., D. Qin, M. Manning, Z. Chen, M. Marquis, K.B. Avery, M. Tingor, and H.L. Miller (eds.), Cambridge University Press, Cambridge, United Kingdom and New York, NY, USA.

Mernild, S.H., G.E. Liston, C.A. Hiemstra, and J.H. Christensen (2010), Greenland Ice Sheet surface mass-balance modeling in a 131-year perspective, 1950-2080, *Journal of Hydrometeorology*, *11*, 1, 3-25.

Mikolajweicz, U., M. Vizcaíno, J. Jungclaus, and G. Schurgers (2007), Effect of ice sheet interactions in anthropogenic climate change simulations, *Geophys.Res.Lett.*, *34*, L18706, doi:10.1029/2007GL031173.

Mitchell, T.D. and P.D. Jones (2005), An improved method of constructing a database of monthly climate observations and associated high-resolution grids, *Int.J.Climatol.*, *25*, 693712.

Mottram, R., et al. (2012), A new analysis of Surface Mass Balance for the Greenland Ice Sheet 1989 - 2011 from HIRHAM5, in preparation, to be submitted to *The Cryosphere*.

Nakicenovic, N., Alcamo, J., Davis, G., de Vries, B., Fenhann, J., Gaffin, S., Gregory, K., Grübler, A., Jung, T.Y., Kram, T., La Rovere, E.L., Michaelis, L., Mori, S., Morita, T., Pepper, W., Pitcher, H., Price, L, Riahi, K., Roehrl, A., Rogner, H.-H., Sankovski, A., Schlesinger, M., Shukla, P., Smith, S., Swart, R., van Rooijen, S., Victor, N. and Zhou, D. (2000), *IPCC Special Report on Emissions Scenarios*, Cambridge University Press, Cambridge, UK. Available at: `http://www.grida.no/publications/other/ipcc_sr/?src=/climate/ipcc/emission/`

Reeh, N. (1991), Parameterization of melt rate and surface temperature on the Greenland ice sheet, *Polarforschung*, it59, 113-128.

Ridley, J.K., P. Huybrechts, J.M. Gregory, J.A. Lowe (2005), Elimination of the Greenland ice sheet in a high CO2 climate, *J.Clim.*, *18*, 17, 3409-3427.

Rignot, E., et al. (2008), Mass balance of the Greenland ice sheet from 1958 to 2007, *Geophys. Res. Lett.*, *35*, L20502.

Roeckner, E., G. Bäuml, L. Bonaventura, R. Brokopf, M. Esch, M. Giorgetta, S. Hagemann, I. Kirchner, L. Kornblueh, E. Manzini, A. Rhodin, U. Schlese, U. Schulzweida and A. Tompkins (2003), *The atmospheric general circulation model ECHAM 5. Part I: Model description*, Max-Planck-Institut für Meteorologie, Hamburg, Germany, 126pp

Stendel, M., J.H. Christensen, and D. Petersen (2008), Arctic climate and climate change with a focus on Greenland, In: Meltofte, H., T.R. Christensen, B. Elberling, M.C. Forchhammer, and M. Rasch (eds.): High Arctic Ecosystem Dynamics in a Changing Climate. Ten years of monitoring and research at Zackenberg Research station, Norheast Greenland. Advances in Ecological Research. *Advances in Ecological Research*, Academic Press, *40*, 13-43.

Undén, P., et al.(2002), *High Resolution Limited Area Model, HiRLAM-5 scientific documentation*, Tech. rep., Swed. Meteorol. and Hydrol. Inst., Norrköping, Sweden.

van de Berg, W.J., M.R. van den Broeke, and E. van Meijgaard (2012), Quantifying the uncertainty in model-based estimates estimate of ice sheet surface mass balance, to be submitted to *The Cryosphere*.

Van de Wal, R.S.W., W. Greuell, M.R. van den Broeke, C.H. Reijmer and J. Oerlemans (2005), Surface mass-balance observations and automatic weather station data along a transect near Kangerlussuaq, West Greenland, *Ann.Glaciol.*, *42* (1), 311-316.

Van Meijgaard, E., et al. (2008), *The KNMI regional atmospheric climate model RACMO version 2.1*, Tech. Rep. 302.

Vizcaíno, M., U. Mikolajweicz, M. Gröger, E. Maier-Reimer, G. Schurgers, and A.M.E. Winguth (2008), Long-term ice sheet-climate interactions under anthropogenic greenhouse forcing simulated with a complex Earth System Model, *Clim.Dyn.*, *31*, 665-690.

Vizcaíno, M., U. Mikolajweicz, J. Jungclaus, and G. Schurgers (2010), Climate modification by future ice sheet changes and consequences for ice sheet mass balance, *Clim.Dyn.*, *34*, 301-324.

Wake, L.M., P. Huybrechts, J.E. Box, E. Hanna, I. Janssens, G.A. Milne (2009), Surface mass-balance changes of the Greenland ice sheet since 1866, *Ann.Glaciol.*, *50*, 178-184.

White, P.W. (ed.) (2004), *IFS documentation CY23R4: Part IV physical processes* (see `http://www.ecmwf.int/research/ifsdocs`).

Met Office
FitzRoy Road, Exeter
Devon, EX1 3PB
UK

Tel: 0870 900 0100
Fax: 0870 900 5050
enquiries@metoffice.gov.uk
www.metoffice.gov.uk